Published online 25 June 2018

Nucleic Acids Research, 2018, Vol. 46, No. 15 ***7643–7661***
doi: 10.1093/nar/gky535

Post-transcriptional regulation of *Pabpn1* by the RNA binding protein HuR

Brittany L. Phillips[1,2,3], Ayan Banerjee[1], Brenda J. Sanchez[4], Sergio Di Marco[4], Imed-Eddine Gallouzi[4,5], Grace K. Pavlath[2,*] and Anita H. Corbett[1,*]

[1]Department of Biology, Emory University, Atlanta, GA 30322, USA, [2]Department of Pharmacology, Emory University School of Medicine, Atlanta, GA 30322, USA, [3]Genetics and Molecular Biology Graduate Program, Emory University, Atlanta, GA 30322, USA, [4]Department of Biochemistry, Goodman Cancer Center, McGill University, Montreal, Quebec, Canada and [5]Hamad Bin Khalifa University (HBKU), Life Sciences Division, College of Sciences and Engineering, Education City, Doha, Qatar

Received January 16, 2018; Revised May 23, 2018; Editorial Decision May 26, 2018; Accepted June 08, 2018

ABSTRACT

RNA processing is critical for proper spatial and temporal control of gene expression. The ubiquitous nuclear polyadenosine RNA binding protein, PABPN1, post-transcriptionally regulates multiple steps of gene expression. Mutations in the *PABPN1* gene expanding an N-terminal alanine tract in the PABPN1 protein from 10 alanines to 11–18 alanines cause the muscle-specific disease oculopharyngeal muscular dystrophy (OPMD), which affects eyelid, pharynx, and proximal limb muscles. Previous work revealed that the *Pabpn1* transcript is unstable, contributing to low steady-state *Pabpn1* mRNA and protein levels *in vivo*, specifically in skeletal muscle, with even lower levels in muscles affected in OPMD. Thus, low levels of PABPN1 protein could predispose specific tissues to pathology in OPMD. However, no studies have defined the mechanisms that regulate *Pabpn1* expression. Here, we define multiple *cis*-regulatory elements and a *trans*-acting factor, HuR, which regulate *Pabpn1* expression specifically in mature muscle *in vitro* and *in vivo*. We exploit multiple models including C2C12 myotubes, primary muscle cells, and mice to determine that HuR decreases *Pabpn1* expression. Overall, we have uncovered a mechanism in mature muscle that negatively regulates *Pabpn1* expression *in vitro* and *in vivo*, which could provide insight to future studies investigating therapeutic strategies for OPMD treatment.

INTRODUCTION

RNA processing ensures proper spatial and temporal control of gene expression. RNA binding proteins are critical for every aspect of RNA processing from 5′ capping and 3′ end formation in the nucleus to eventual RNA turnover in the cytoplasm. Consistent with the critical roles for RNA binding proteins in gene expression, the vast majority of these proteins are ubiquitously expressed (1). Despite this ubiquitous requirement for RNA binding proteins, mutations in genes encoding RNA binding proteins often cause tissue-specific disease (2). The molecular deficiencies underlying tissue-specificity are typically difficult to define and likely depend on the functions of the RNA binding protein as well as the context and specific requirements within the affected tissue. Interestingly, mutations in genes encoding RNA binding proteins often affect nervous and muscle tissue (2), suggesting that these complex tissues have strict requirements for proper RNA processing and control of gene expression. One example of an RNA binding protein linked to a tissue-specific disease is the polyadenylate binding protein nuclear 1 (PABPN1). Mutations in the ubiquitously-expressed *PABPN1* gene cause the muscle-specific disease oculopharyngeal muscular dystrophy (OPMD) (3).

Although PABPN1 regulates multiple aspects of RNA processing (4), the best characterized role for PABPN1 is controlling poly(A) tail length by stimulating poly(A) polymerase (5,6). More recent work has defined how PABPN1 and polyadenylation serve as quality control mechanisms. Depletion of *Pabpn1* causes global poly(A) tail shortening and nuclear poly(A) RNA retention in primary muscle cells, demonstrating that PABPN1-mediated RNA processing events are necessary for efficient RNA nuclear export (7). Furthermore, PABPN1 and poly(A) polymerase hyperadenylate improperly spliced or intron-retaining RNAs, targeting these RNAs for exosome-mediated degradation (8). PABPN1 also modulates alternative polyadenylation (9–13), demonstrating that PABPN1 regulates 3′ untranslated region (3′UTR) length which could influence downstream post-transcriptional regulatory mechanisms. Thus,

*To whom correspondence should be addressed. Tel: +1 404 727 4546; Email: acorbe2@emory.edu
Correspondence may also be addressed to Grace K. Pavlath. Email: gpavlat@emory.edu

PABPN1 plays critical roles in numerous RNA processing events important for proper gene expression.

In addition to a conventional RNA recognition motif (RRM) (14) that mediates RNA binding, the PABPN1 protein contains a 10-alanine tract immediately following the initial methionine (3) in a region of the protein with no characterized function. Patients with OPMD have GCN triplet expansion mutations that extend this 10-alanine tract to 11–18 alanines (3). How this subtle expansion in a region of the PABPN1 protein with no known function causes an autosomal dominant disease affecting a specific subset of muscles in the eyelid, pharynx and proximal limbs is not understood.

Studies aimed at understanding how this modest alanine expansion in PABPN1 confers pathology in a subset of skeletal muscles have typically focused on the propensity of alanine-expanded PABPN1 to form insoluble nuclear aggregates (13,15,16). Aggregate-positive myonuclei from a transgenic mouse model overexpressing expanded PABPN1 are positive for cell death markers (17), suggesting that this alanine tract expansion may induce toxicity. However, both wildtype and expanded PABPN1 can aggregate *in vitro,* and this aggregation does not require the N-terminus containing the alanine tract (18). Furthermore, nuclear aggregates are only present in ∼5% of myonuclei (16) and be detected in rat neurons (19,20) and OPMD patient brain sections (21), a cell type/tissue that is not typically affected in patients with OPMD (4). These observations raise questions about whether aggregate-driven toxicity is the sole mechanism of pathology in OPMD.

Aggregate-mediated disease pathology would logically occur in tissues with high levels of the mutant protein. If toxic PABPN1 aggregates were the sole source of pathology in OPMD, tissues that express high levels of the toxic protein would likely be the most susceptible to pathology. However, PABPN1 levels are extremely low in skeletal muscles compared to other tissues not affected in OPMD (22). In fact, PABPN1 protein levels are even lower in muscles that are typically affected in OPMD patients such as pharynx than other skeletal muscles (22). These low PABPN1 levels may predispose particular muscles to OPMD pathology.

As PABPN1 levels are low in muscle, a reduction in the functional pool of PABPN1 protein may more severely affect muscle than tissues with higher PABPN1 levels. Thus, in OPMD, functional PABPN1 levels may fall below a threshold for pathology only in muscle while non-muscle tissues have sufficient levels of functional PABPN1 to fulfill tissue-specific requirements (22). Immunofluorescence studies have identified PABPN1 as well as other proteins sequestered in insoluble aggregates in OPMD patient muscle tissue (23,24), and overexpression studies have identified specific RNAs present in these aggregates (25). Thus, aggregation could cause or contribute to a decrease in the functional pool of PABPN1 in muscle where levels of PABPN1 are already low compared to other tissues. Together, these observations suggest a more complex disease pathology than purely aggregate-mediated toxicity. Therefore, increasing PABPN1 protein levels in muscles typically affected by PABPN1 expansion could be protective and considered as a component of future OPMD therapies. Unfortunately, little is known about any mechanisms that regulate expression of *PABPN1*.

The bulk of muscle-specific regulation of PABPN1 levels occurs at the RNA level as steady-state *Pabpn1* mRNA levels are low in muscle *in vivo* (22). Furthermore, the *Pabpn1* transcript is highly unstable in muscle relative to non-muscle tissue *in vivo*, demonstrating that *Pabpn1* transcript instability contributes to low PABPN1 protein levels that are observed in muscle (22). Defining the mechanisms that regulate the *Pabpn1* transcript in muscle may identify novel targets that modulate PABPN1 protein levels.

To interrogate the specific mechanisms regulating the *Pabpn1* transcript, we combined the strengths of an *in vitro* model of mature skeletal muscle, C2C12 myotubes, with *in vivo* analyses. Here we validate C2C12 myotubes as an *in vitro* model of skeletal muscle in which to define the mechanisms that regulate *Pabpn1* in muscle. We define *cis*-regulatory elements in the *Pabpn1* 3′UTR including an AU-rich element (ARE) bound by the RNA binding protein HuR. We identify HuR as a post-transcriptional regulator of *Pabpn1* transcript and protein levels. Furthermore, HuR-mediated *Pabpn1* regulation is conserved *in vivo* in muscles and primary muscle cells. These data demonstrate that HuR negatively regulates *Pabpn1* at the RNA and protein levels, providing insight into the mechanisms regulating *Pabpn1* expression in a mature skeletal muscle-specific manner. This regulatory mechanism could be exploited as a novel therapeutic approach to increase PABPN1 protein levels in OPMD.

MATERIALS AND METHODS

Cell culture

Although most experiments utilize the mouse myoblast cell line C2C12 (ATCC CRL-1772), we have also used mouse fibroblasts (NIH/3T3, ATCC CRL-1658), human embryonic kidney cells (HEK293, ATCC CRL-1573) and primary myoblasts harvested from murine hindlimb muscles for particular experiments. Cultured cells were maintained in a humidified incubator with 5% CO_2 at 37°C. Mouse C2C12 myoblasts were cultured in C2C12 growth media (Dulbecco's modified Eagle's medium [DMEM] with 4.5 g/l glucose, 10% FBS, 100 U/ml penicillin, 100 U/ml streptomycin). To induce C2C12 differentiation, C2C12 myoblasts were plated on dishes coated with Entactin—Collagen IV—Laminin (ECL; Upstate Biotechnology) in C2C12 differentiation media which was changed every other day. The majority of experiments utilized a 6-day differentiation protocol in which cells were differentiated in DMEM with 4.5 g/l glucose, 1% horse serum, 100 U/ml penicillin, 100 U/ml streptomycin. For one northern blotting experiment (Figure 3D), C2C12 myoblasts were differentiated using a 10-day differentiation protocol (DMEM with 1 g/l glucose, 1% horse serum, 100 U/ml penicillin, 100 U/ml streptomycin). Mouse NIH/3T3 fibroblasts and HEK293 cells were cultured in DMEM with 4.5 g/l glucose supplemented with 10% FBS, 100 U/ml penicillin, and 100 U/ml streptomycin.

Primary myoblasts were isolated from control ($HuR^{fl/fl}$) and *HuR*-knockout ($HuR^{\Delta/\Delta}$) hindlimb muscles (Gallouzi *et al.*, unpublished data) from three male 3-month-old mice

per genotype using a protocol yielding cultures >95% myogenic (26). Briefly, muscles were dissected, minced and digested with 0.1% pronase (EMD Millipore) for 1 h at 37°C with mild agitation. The digested material was triturated and filtered through a 100 μm vacuum filter (EMD Millipore). Primary myoblasts were plated on collagen-coated (Bovine Collagen I, Gibco) dishes in primary growth media (Ham's F10, 20% FBS, 5 ng/ml bFGF, 100 U/ml penicillin, 100 U/ml streptomycin). To induce differentiation, primary myoblasts were plated on dishes coated with ECL in primary differentiation media (DMEM with 1 g/l glucose, 1% Insulin—Transferrin—Selenium-A [ITS] supplement [Invitrogen], 100 U/ml penicillin, 100 U/ml streptomycin). Primary myotubes were harvested after 36–48 h in differentiation media as indicated.

Immunoblotting

Cells were lysed and muscles homogenized using standard methods (7). After lysis/homogenization, samples were sonicated at 30% output for 10s to shear chromatin (Branson Sonifier 250, VWR Scientific). Protein concentrations were determined using a Bradford assay (BioRad), and equal amounts of protein were boiled in reducing sample buffer (250 mM Tris–HCl pH 6.8, 500 mM DTT, 10% SDS, 0.5% Bromophenol Blue, 50% glycerol) and resolved using 4–20% Criterion TGX polyacrylamide gels (BioRad). Fractionation protein samples were resolved using 4–20% Criterion TGX Stain-Free polyacrylamide gels (BioRad), which were UV-activated using the ChemiDoc MP Imaging System (BioRad) according to the manufacturer's instructions. Proteins were transferred to 0.2 μm nitrocellulose membranes and these membranes were stained with Ponceau S Solution (Sigma-Aldrich) to assess the amount of total protein loaded across samples. Membranes were then blocked in 10% nonfat dry milk in Tris-buffered saline pH 7.4 with 0.1% Tween-20 (TBS-T). Primary antibodies were diluted in 5% nonfat milk in TBS-T and incubated overnight at 4°C. Species-specific horseradish peroxidase conjugated secondary α-IgG antibodies (Jackson ImmunoResearch Laboratories) were used to detect primary antibodies, followed by enhanced chemiluminescence substrate (ECL, Sigma). Chemiluminescence was detected by exposing blots to autoradiography film or using the ChemiDoc MP Imaging System (BioRad). Multiple exposures were taken to ensure all analyses were performed in the linear range of the signal. The following antibody concentrations were used: α-PABPN1 (1:4000) (7), α-HuR (3A2, 1:10,000) (27), α-eMyHC F1.652 (1:100, Developmental Studies Hybridoma Bank, Iowa City, Iowa) (28), α-Histone H3 (1:20,000, Abcam), α-KSRP (1:2000, Bethyl Labs), α-CUGBP1 (1:1500, Bethyl Labs), α-HSP90 (1:5000, Santa Cruz), α-GAPDH (1:1000, Bethyl Labs) and α-MATR3 (1:4000, Bethyl Labs). Immunoblot signals within the linear range of detection and Ponceau staining were quantified using ImageJ software. To normalize protein loading for all immunoblotting experiments except for fractionation immunoblots, Ponceau stain was quantified across a region of the membrane with similar staining patterns for all lanes. Nuclear (MATR3) or cytoplasmic (GAPDH) protein was quantified using ImageJ to normalize protein loading for fractionation immunoblots.

RNA preparation, cDNA and qRT-PCR

Total RNA was isolated using TRIzol reagent (ThermoFisher Scientific) and treated with DNase I, Amplification Grade (Invitrogen) according to the manufacturer's instructions. cDNA was synthesized using the M-MLV reverse transcriptase kit (Invitrogen) and Rnasin (Promega). Approximately 10 ng of cDNA was mixed with appropriate primers and SYBR Select Master Mix (Applied Biosciences) for qRT-PCR analysis. Samples were analyzed using the comparative Ct method (29) on an Applied Biosciences Step One Real Time PCR System. Samples were normalized to *Gapdh* or *Hprt*, which have been used previously for normalization in studies of muscle and muscle cells (22,30) and NIH/3T3 cells (31), as indicated. To identify appropriate normalizer transcripts for each experiment, we performed analyses to ensure no significant changes across the samples and conditions employed were detected (Supplementary Figures S1 and S2A–C). We calculated the level of normalizer transcript detected in all samples per experiment using the 2^{-Ct} method. As shown in Supplementary Figure S1A, the Ct value was converted using the 2^{-Ct} method and levels were assessed by dividing this value by the total value detected for that transcript across samples. Specifically, we summed 2^{-Ct} values combining values for all samples. The 2^{-Ct} value for each individual sample was then divided by the total amount detected across samples and multiplied by 100 to yield a Percentage of that transcript in the specific sample relative to the total amount of that transcript detected across all samples. Transcripts with no significant change in level (as a percentage of that transcript relative to total for that transcript across all samples analyzed) across samples analyzed were employed for normalization in all experiments as indicated for individual experimental results. For example, Supplementary Figure S1 shows this analysis for the *Gapdh* transcript comparing C2C12 myoblasts (MB) and myotubes (MT). For eleven total samples in two independent experiments (5 MB and 6 MT), we used qRT-PCR to assess levels of *Gapdh* transcript as assessed by 2^{-Ct} value. For each individual measurement (Supplementary Figure S1A), we divided that 2^{-Ct} value by the total summed 2^{-Ct} values for all samples (eleven samples). Supplementary Figure S1B compares the Ct values while Supplementary Figure S1C plots the percentage of total that each individual 2^{-Ct} value represents of the total value calculated for all 2^{-Ct} values. The data were analyzed in the same manner for MB and MT, but they are shown separately to indicate both the consistency in *Gapdh* transcript levels within a sample (MB) but also across different samples (compare values for MB to MT). A similar approach was taken for all transcripts employed to normalize qRT-PCR samples in all experiments.

RNA stability assay

Cells were treated with 5 μg/ml Actinomycin D to inhibit transcription. Because long term Actinomycin D treatment can impact cell physiology and confound results from stability assays, we chose appropriate time points that have been

previously validated for NIH/3T3 cells (31) and C2C12 myoblasts and myotubes (30). We did not detect a change in viability with this 8h time course in any cell type analyzed. C2C12 and NIH/3T3 cells were lysed after 30 min, 1 h, 2 h, 4 h, 6 h and 8 h following Actinomycin D treatment. RNA was isolated and reverse transcribed as previously described. Transcript levels were determined using qRT-PCR and normalized to levels of *Gapdh* for C2C12, and *Hprt* for NIH/3T3 cells. Fold change was calculated relative to *Pabpn1* levels at the 30 min time point for C2C12 myoblasts and myotubes and NIH/3T3 cells. Each data point representing the mean of 3–4 individual experiments (32) was plotted and appropriately fitted lines/curves corresponded with reasonable correlation coefficients ($R^2 > 0.9$). For the *Pabpn1* transcript in C2C12 myotubes, linear regression was conducted using GraphPad Prism to calculate the slope and the decay rate constant (k) and mRNA half-life was calculated using the equation $t_{1/2} = \ln(2)/k$ (33). For the *Myc* transcript, RNA half-life was quantified with GraphPad Prism using a one-phase decay equation to fit a nonlinear regression curve to plotted data. As described in detail under the 'RNA preparation, cDNA, and qRT-PCR' section above, to identify appropriate normalizer transcripts that do not decay over the course of this experiment, we calculated the amount of normalizer transcript detected in all samples per experiment using the 2^{-Ct} method. For each experiment, the Ct value was converted using the 2^{-Ct} method and amount per sample was assessed by dividing this value by the total value detected for that transcript across samples. We summed 2^{-Ct} values combining values for all samples per experiment. The 2^{-Ct} value for each sample was then divided by the total amount detected across samples and multiplied by 100. Transcripts with no significant change in level at time points assessed were determined to be appropriate normalizer transcripts (Supplementary Figure S2A–C).

Sequence alignment

Sequences were obtained from the UCSC Genome Browser (34) for the human (December 2013, GRCh38/hg38) (35), bovine (June 2014, Bos_taurus_UMD_3.1.1/bosTau8) (36) and murine (December 2011, GRCm38/mm10) (35) *Pabpn1* 3′UTRs. Sequences were aligned using DNASTAR MegAlign Pro with the MUSCLE alignment algorithm. Uncorrected pairwise distance was used to determine the distance of human, bovine, and murine *Pabpn1* 3′UTRs (Supplementary Figure S3A) with global gap removal and 841 residues considered. Percent identity relative to human *Pabpn1* 3′UTR was calculated as %ID = 100 × (1 – distance).

Defining polyadenylation site (PAS) utilization

Primers were designed to amplify regions within the coding DNA sequence (CDS) and the region between the proximal and distal PAS (distal). PAS usage was quantified by calculating the ΔΔCt as distal minus CDS after *Gapdh* normalization (13). Fold change is presented as a ratio relative to the average fold change from C2C12 myoblast samples.

Northern blotting

Total RNA from tissues and cells was isolated as described above under, 'RNA preparation, cDNA and qRT-PCR.' RNA (20 μg) was loaded on a 1.4% agarose denaturing formaldehyde gel. RNA was transferred to Amersham Hybond-N+ membrane (GE Healthcare and Life Sciences) with 10× SSC buffer. RNA was UV-crosslinked and prehybridized at 65°C in 100 μg/ml salmon sperm DNA (Invitrogen) in Rapid-Hyb buffer (GE Healthcare Life Sciences). PCR using primers spanning exons 2–3 (forward primer) and exons 6–7 (reverse primer) generated an ∼400 nucleotide *Pabpn1* probe (22). This *Pabpn1* PCR product was [α-^{32}P]dCTP (Perkin Elmer) labeled using the Amersham RediPrime II DNA Labelling System (GE Healthcare Life Sciences) and purified with illustra MicroSpin G-25 columns (GE Healthcare Life Sciences). The *Pabpn1* probe was hybridized to the membrane rotating at 65°C overnight. The reverse *18S* oligo was end-labeled with [γ-^{32}P]dATP (Perkin Elmer) using PNK (New England Biolabs) and purified with illustra MicroSpin G-25 columns (GE Healthcare Life Sciences). The *18S* probe was hybridized rotating at 42°C overnight. A Typhoon phosphorimager or autoradiography film were used to detect labeled probe. The rRNA *18S* films were exposed for 1 h while *Pabpn1* films were exposed for ∼50 h. Northern blots were quantified using ImageJ software. The band for *18S* rRNA was used to normalize RNA loading.

Plasmids

The sequence for the murine *Pabpn1* 3′UTR was synthesized (GeneArt) and XhoI/XbaI digestion was used to insert the fragment into the pcDNA3 luciferase vector (37) by the Emory Integrated Genomics Core (EIGC). Site-directed mutagenesis was used to delete the first polyadenylation site (PASI, 5′-ATTAAA-3′), termed ΔPASI. The ΔPASI 3′UTR construct was used as a template for site-directed mutagenesis to disrupt AREs by mutating thymines to guanosines (38,39). This mutation scheme was used to generate two mutated *Pabpn1* 3′UTR plasmids: one plasmid with mutations disrupting ARE1, and a separate plasmid with mutated ARE4 where thymines that are conserved within the consensus HuR CLIP site (40,41) from mice to humans were mutated. The ΔPASI 3′UTR construct was also used to generate three separate plasmids with a deleted ARE2, ARE3 and ARE4, respectively. The pGEM-Teasy *GAPDH* 3′UTR (pGEM-Teasy) plasmid was previously described (42).

RNA immunoprecipitation (RIP)

To investigate interactions between HuR and target mRNAs, RNA immunoprecipitation (RIP) was performed on C2C12 myotube lysate according to standard methods (43,44). Briefly, C2C12 myotubes grown in a 150 cm dish were rinsed twice with ice-cold PBS and lysed with an equal pellet volume of RIPA-2 buffer [50 mM Tris, pH 7.4, 150 mM NaCl, 0.1% SDS, 1% Triton X-100, 1% Na-deoxycholate, 1 mM EDTA and 1 cOmplete protease inhibitor tablet (Sigma)]. Protein-A Dynabeads (Invitrogen) were incubated with either mouse IgG or HuR antibody

(27). Beads coated in antibody were resuspended in NT2 buffer (50 mM Tris–HCl, pH 7.4, 150 mM NaCl, 1 mM $MgCl_2$, 0.05% Nonidet P-40 with Rnasin [Promega] and 1 mM DTT). Thawed and clarified lysates were added and the bead/antibody/lysate mixture was incubated at 4°C overnight rotating end-over-end. Beads were washed with cold NT2 buffer five times. Proteinase K treatment released RNAs from bound proteins and input and bound RNA was isolated with TRIzol (Invitrogen) and reverse transcribed as described above. Enrichment for *Pabpn1* and *Gapdh* transcripts with HuR immunoprecipitation was calculated using the comparative Ct method (29), with samples normalized to input and compared to IgG control. Data are presented as fold enrichment relative to *Gapdh* enrichment for each sample.

Biotin RNA affinity purification

All *Pabpn1* 3′UTR PCR products generated for use in *in vitro* transcription reactions were amplified from firefly luciferase constructs described in the, 'Plasmids' section above. To analyze HuR interaction with the *Pabpn1* 3′UTR (Figure 4C), we utilized a construct containing the wildtype murine *Pabpn1* 3′UTR downstream of firefly luciferase. The *Pabpn1* 3′UTR was amplified using PCR with a forward primer containing the T7 promoter. A pGEM-Teasy vector containing the wildtype human *GAPDH* 3′UTR with a T7 promoter (42) was linearized by *SpeI* digestion (New England Biolabs) and gel purified. For experiments determining the region of HuR interaction with the *Pabpn1* 3′UTR (Figure 5B), we used T7 primers to amplify the *Pabpn1* 3′UTR from the following firefly luciferase constructs: ΔPASI murine *Pabpn1* 3′UTR with a deleted PASI, and mutARE4 murine *Pabpn1* 3′UTR with a deleted PASI and mutated ARE4.

DNA template (1 μg) was used for *in vitro* transcription. Biotinylated RNAs were generated with the T7 MAXIscript Kit (ThermoFisher Scientific) with biotin-16-UTP (Roche) according to the manufacturer's instructions in the presence of Rnasin (Promega). Biotinylated RNAs were purified with illustra MicroSpin G-25 columns (GE Healthcare Life Sciences). Biotinylated RNA size and integrity was confirmed using RNA gel electrophoresis (Supplementary Figure S5), which was also used to confirm equal RNA quantification for experiments comparing ΔPASI *Pabpn1* 3′UTR and mutARE4 *Pabpn1* 3′UTR biotinylated RNAs (Supplementary Figure S6). To reduce nonspecific binding, Streptalon streptavidin magnetic beads (bioWORLD) were blocked in 4 mg/ml BSA (Sigma) in IP buffer (50 mM Tris–HCl, pH 7.5, 150 mM NaCl, 5 mM $MgCl_2$, 0.5 mM DTT, 1% Nonidet P-40 supplemented with cOmplete protease inhibitor tablets [Roche Applied Science]) for 3 h at 4°C rotating end-over-end. Beads were then incubated with 400 ng biotinylated RNA and Rnasin (Promega) for 20 min at 4°C rotating end-over-end.

To prepare lysate, C2C12 myotubes were lysed in IP buffer, sonicated twice for 10 s at 30% output (Branson Sonifier 250, VWR Scientific), and centrifuged at 21 000 × g for 20 min at 4°C. A total of 400 μg of protein lysate per sample was pre-cleared with washed beads rotating end-over-end at room temperature for 20 min. Lysate, biotinylated RNA, and beads were incubated at room temperature rotating end-over-end for 20 min. Beads were washed five times with cold IP buffer and proteins were eluted by boiling for 5 min in reducing sample buffer. Input and bound proteins were resolved by SDS-PAGE using 4–20% Criterion TGX polyacrylamide gels (BioRad) and analyzed by immunoblotting.

Firefly luciferase assays

C2C12 myoblasts were plated and differentiated in 96-well plates for luciferase assays. On differentiation day 5, myotubes were transfected with luciferase reporter plasmids using DNA-In CRISPR reagent (Amsbio) according to the manufacturer's instructions in the absence of antibiotics. Media was changed 16h after transfection. For primary myoblast luciferase assays, primary myoblasts were plated in differentiation media and reverse transfected with luciferase reporter plasmids using DNA-In CRISPR reagent (Amsbio) according to the manufacturer's instructions in the absence of antibiotics. Media was changed 16 h after transfection. Luciferase assays were conducted using the Dual-Luciferase Reporter Assay System (Promega). Cells were lysed 24 h (C2C12 myotubes) or 48 h (primary myotubes) after transfection according to the manufacturer's instructions. A BioTek Microplate reader was used to measure luminescence with a 2 s delay and 2 s integration time. Renilla luciferase (pRL-CMV [Promega]) activity was used to normalize firefly luciferase activity. Data are presented as the ratio of firefly to renilla luciferase activity relative to ΔPASI control for three independent experiments.

siRNA knockdown

Standard siRNA knockdown was employed to deplete HuR. siRNA transfections were conducted using Lipofectamine 2000 (Invitrogen). The following siRNAs were used at a final concentration of 100 nM: Low GC negative control (Invitrogen), HuR Stealth RNAi MSS205315 (Invitrogen) referred to as siRNA HuR#1, HuR Stealth RNAi MSS205313 (Invitrogen) referred to as siRNA HuR#2, HuR Stealth RNAi MSS205314 (Invitrogen) referred to as siRNA HuR#3. C2C12 myotubes were transfected with a single siRNA in the absence of antibiotics on the third day of differentiation (differentiation day 3). Media was changed 16 h after transfection. To enhance HuR depletion, a second knockdown was conducted 24 h after the first transfection (differentiation day 4). Cells were harvested 72 h after the initial transfection (differentiation day 6). Immunoblotting was performed to confirm knockdown, and qRT-PCR was conducted to assess changes in steady-state *Pabpn1* transcript levels with *HuR* knockdown.

Cellular fractionation

C2C12 myoblasts and myotubes were fractionated using standard methods (45). Briefly, cells were scraped in ice-cold PBS and centrifuged at 1000× g for 5 min. Cell pellets were resuspended in lysis buffer (10 mM Tris, pH 8.0, 140 mM NaCl, 1.5 mM $MgCl_2$, 0.5% Nonidet P-40, 2 mM vanadyl ribonucleoside complex [VRC]) and incubated on

ice for 5 min. Lysate was centrifuged at 1000 × g for 3 min at 4°C to pellet nuclei. The supernatant was collected as cytoplasm and cleared by centrifugation at 13 000 rpm for 10 min at 4°C. The nuclear pellet was washed twice and resuspended in lysis buffer. To account for differences in cytoplasmic morphology between myoblasts and myotubes, equal amounts of total protein (7.5 μg) were analyzed by immunoblot.

Animals

All mice are from the C57Bl/6J background. Muscle-specific HuR knockout ($HuR^{\Delta/\Delta}$) mice were generated by crossing $HuR^{fl/fl}$ mice containing loxP sites flanking exon 2 of the *HuR* gene with mice containing the Cre recombinase gene under the control of the *MyoD* promoter (Gallouzi *et al.*, unpublished data). All experiments used muscle tissue from 3-month-old male mice in biological triplicate per genotype. Rectus femoris and gastrocnemius muscles were used for immunoblotting experiments. Hindlimb muscles including rectus femoris, gastrocnemius, soleus and tibialis anterior muscles were harvested for primary myoblast isolation. Primary myoblasts were isolated from three animals per genotype and treated as independent biological samples. Testing for rodent-related pathogens was routinely performed by McGill University's Comparative Medicine and Animal Resources Center. Animal experiments were approved by the McGill University Faculty of Medicine Animal Care Committee and in accordance with the guidelines set by the Canadian Council of Animal Care.

Data analysis

For the majority of experiments, raw data are normalized to the appropriate values (Ponceau stain for immunoblots, *Gapdh*/*Hprt* for qRT-PCR, renilla luciferase activity for luciferase assays, etc.) as indicated. The average normalized values for control samples (C2C12 myoblasts, $HuR^{fl/fl}$cells, etc.) was set to 1.0, and all data are presented as values relative to this mean.

Statistical analysis

For all experiments, statistical analyses were performed using GraphPad Prism. For RNA decay analysis, RNA decay normalizer analysis, and primary myotube luciferase assays, one-way analysis of variance (ANOVA) was conducted. Student's t-test was used for all other experiments. In all cases, $P < 0.05$ is considered statistically significant.

RESULTS

Steady-state *Pabpn1* mRNA and protein levels are low in an *in vitro* model of skeletal muscle

Our previous studies revealed that *Pabpn1* mRNA and protein are present at very low levels in both mouse and human skeletal muscle tissue (22). However, investigating the mechanisms underlying this regulation of *Pabpn1* expression in tissue is challenging. For example, identifying and defining *cis*-elements and *trans*-acting factors that influence *Pabpn1* expression *in vivo* would require generation of multiple mouse models. Therefore, identifying an appropriate and tractable *in vitro* cell culture model is necessary to dissect these skeletal muscle-specific mechanisms regulating *Pabpn1* expression.

Previous studies show that proliferative muscle progenitor cells called myoblasts, have higher PABPN1 levels than mature skeletal muscle (22), similar to levels observed in non-muscle tissue (22). Serum deprivation induces myoblasts to form terminally differentiated, multinucleated myotubes, a well-characterized *in vitro* model of mature skeletal muscle. Therefore, to explore if myoblasts and myotubes are appropriate for studying *Pabpn1* regulation *in vitro*, we employed the immortalized mouse myoblast cell line C2C12 (46). We differentiated C2C12 myoblasts (Figure 1A) into multinucleated myotubes and used morphological (Figure 1B) and biochemical analyses (Figure 1C) to confirm efficient differentiation. The late differentiation marker embryonic Myosin Heavy Chain (eMyHC) (47) is readily detected in myotubes but is undetectable in undifferentiated myoblasts (Figure 1C).

We then compared PABPN1 protein levels in C2C12 myoblasts and C2C12 myotubes to determine whether this *in vitro* system recapitulates patterns of PABPN1 expression observed *in vivo* (22). As shown in Figure 1C,D, PABPN1 protein levels decrease ∼40% in C2C12 myotubes relative to C2C12 myoblasts. To investigate whether this myotube-specific reduction in PABPN1 protein levels occurs at the RNA level, we used qRT-PCR to assess steady-state *Pabpn1* transcript levels relative to *Gapdh* transcript levels which do not significantly change between these cell types (Supplementary Figure S1A–C). Steady-state *Pabpn1* mRNA levels are reduced ∼40% in C2C12 myotubes compared to C2C12 myoblasts (Figure 1E), suggesting that the bulk of differential PABPN1 regulation occurs at the level of RNA. These data are consistent with *in vivo* data showing that *Pabpn1* mRNA and protein levels are low in skeletal muscle relative to primary murine myoblasts and non-muscle tissue (22), demonstrating that this *in vitro* system is appropriate for studying the mechanisms that regulate *Pabpn1* expression in mature muscle.

The *Pabpn1* transcript is unstable in an *in vitro* model of skeletal muscle

In vivo studies identified decreased mRNA stability as one mechanism regulating *Pabpn1* mRNA levels in skeletal muscle (22). We investigated whether *Pabpn1* mRNA stability differs between C2C12 myoblasts and myotubes as these myotubes are an *in vitro* model of mature skeletal muscle. To determine whether *Pabpn1* stability changes in a muscle cell- or myotube-specific manner, we also analyzed *Pabpn1* stability in the mouse fibroblast cell line NIH/3T3 (48). For these experiments, we treated cells with the transcriptional inhibitor Actinomycin D (49) and measured *Pabpn1* mRNA levels over time relative to appropriate normalizer transcripts (Supplementary Figure S2A–C) by qRT-PCR to determine the half-life of the *Pabpn1* transcript. As shown in Figure 2, *Pabpn1* mRNA is stable in both NIH/3T3 (Figure 2A) and C2C12 myoblasts (Figure 2B) over the time course examined. In contrast, the *Pabpn1* transcript is unstable

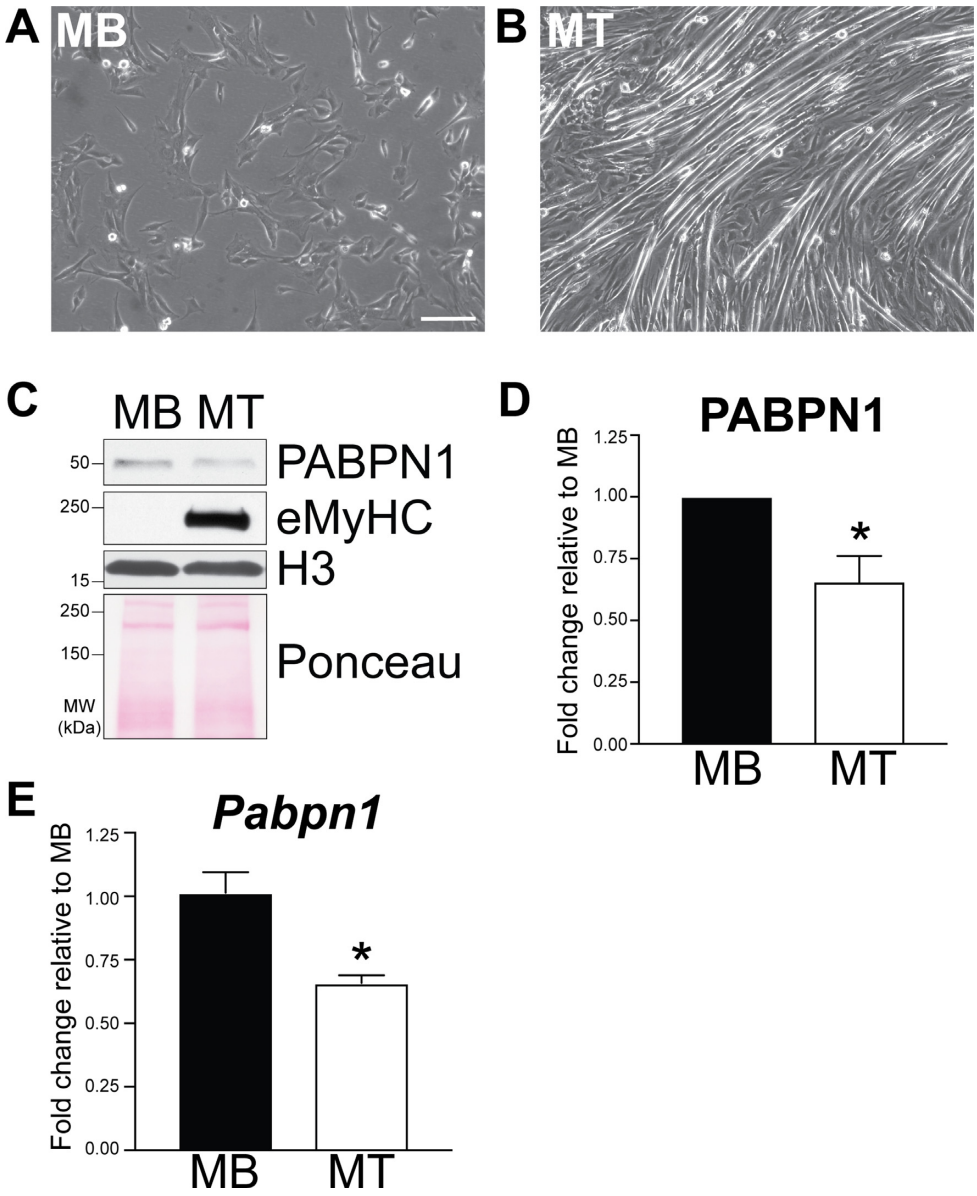

Figure 1. Steady-state *Pabpn1* mRNA and protein levels are low in C2C12 myotubes relative to C2C12 myoblasts. (A, B) Representative images of (**A**) C2C12 myoblasts (MB) and (**B**) C2C12 myotubes (MT) are shown. Bar = 100 μm. (**C**) A representative immunoblot using α-PABPN1 antibody to analyze PABPN1 levels in C2C12 myoblast (MB) and myotube (MT) lysates is shown. The differentiation marker embryonic Myosin Heavy Chain (eMyHC), which is detected only in C2C12 myotube lysate, provides evidence for differentiation. The nuclear protein α-Histone 3 (H3) and Ponceau staining serve as loading controls. (**D**) Quantification of PABPN1 protein levels from three independent immunoblots of lysate prepared from C2C12 myoblasts (MB) and C2C12 myotubes (MT) was performed as described in Materials and Methods. Data were normalized to Ponceau staining as the loading control and are presented as fold change in PABPN1 levels relative to myoblast, which was set to 1.0. Data are mean ± SEM of $n = 3$ independent biological replicates per cell type (*$P < 0.05$). (**E**) qRT-PCR of *Pabpn1* was used to quantify the steady-state levels of *Pabpn1* transcript in total RNA isolated from C2C12 myoblasts (MB) and C2C12 myotubes (MT). Data are presented as fold change relative to average myoblast. For all samples, *Pabpn1* levels were normalized to *Gapdh.* Data presented are mean ± SEM of $n > 5$ independent biological replicates (*$P < 0.05$).

relative to the *Gapdh* transcript in C2C12 myotubes (Figure 2C) relative to both NIH/3T3 and C2C12 myoblasts (Supplementary Figure S2D), with transcript decay first detected at 4h and a projected half-life of ∼13 h. However, because *Gapdh* transcript levels significantly decrease at 8 h in C2C12 myotubes (Supplementary Figure S2C), the extent to which *Pabpn1* decays at this time point cannot be assessed. As a control, *Myc,* a transcript known to be unstable in multiple cell lines and tissue types (50,51), is unstable with a $t_{1/2}$ of ∼0.8 h in all cell lines analyzed (Figure 2, Supplementary Figure S2E). These data demonstrate that the *Pabpn1* transcript is less stable in C2C12 myotubes as compared to NIH/3T3 and C2C12 myoblast cells, illustrating that similar mechanisms could regulate *Pabpn1* expression in C2C12 myotubes and mature muscle tissue.

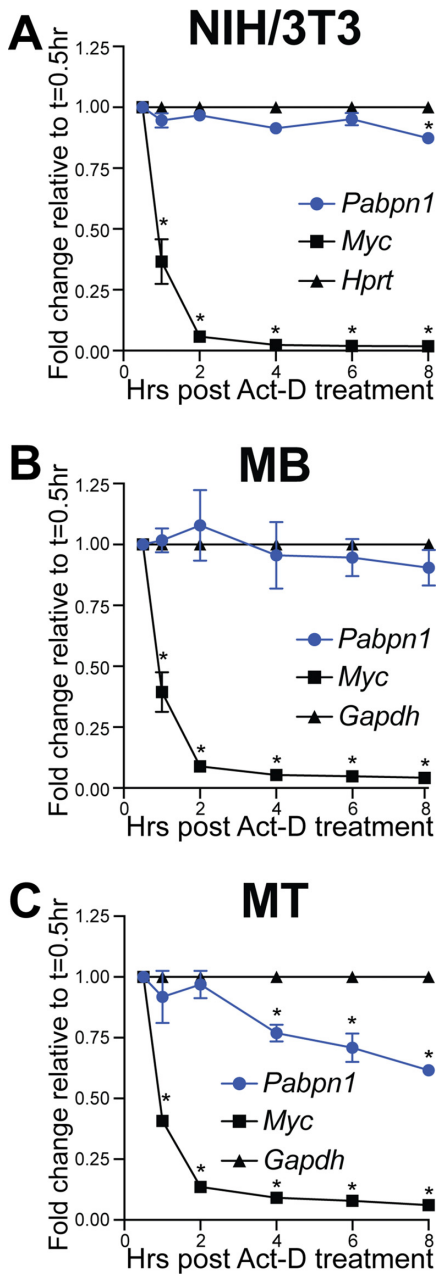

Figure 2. The *Pabpn1* transcript is unstable specifically in C2C12 myotubes. Cells were treated with Actinomycin D (Act-D) to inhibit transcription and total RNA was collected at the indicated time points post-treatment. To assess transcript stability, qRT-PCR was used to detect *Pabpn1* transcript in these samples. *Myc* stability was determined as a control for an unstable transcript. Levels are presented relative to the amount of transcript present at t = 0.5h, which was set to 1.0. For NIH/3T3 cells (**A**), *Pabpn1* and *Myc* levels were normalized to *Hprt*. (**B**) For C2C12 myoblasts (MB) and (**C**) C2C12 myotubes (MT), *Pabpn1* and *Myc* levels were normalized to *Gapdh.* Normalizer transcripts (*Hprt* and *Gapdh*) are set to 1.0 and presented as control stable transcripts on each graph. The calculated half-life of the control unstable *Myc* transcript is ∼0.8h in all cell types tested. Because the *Pabpn1* transcript is stable in NIH/3T3 (A) and C2C12 myoblasts (B) over the course of these experiments, the half-life of the *Pabpn1* transcript in these cells could not be calculated. For C2C12 myotubes (C), the projected half-life of the *Pabpn1* transcript is ∼13 h. Data are presented as mean ± SEM of $n = 3$–4 independent experiments per cell type. ANOVA was conducted to determine if the mean transcript levels (*Pabpn1*, *Myc*) at each time point are statistically significantly different from the mean transcript level detected at $t = 0.5$ h (*$P < 0.05$).

Pabpn1 alternative polyadenylation does not correlate with stability changes

To further investigate myotube-specific *Pabpn1* regulation, we focused on the *Pabpn1* 3′ untranslated region (3′UTR) as 3′UTRs often contain *cis*-regulatory elements that interact with *trans*-acting factors, contributing to spatial and temporal control of gene expression (52). The *Pabpn1* 3′UTR is highly conserved across several mammalian species with bovine and murine *Pabpn1* 3′UTRs sharing 96% and 93% sequence identity within the ∼900 nucleotide human *Pabpn1* 3′UTR, respectively (Supplementary Figure S3A), suggesting that regulatory elements in the *Pabpn1* 3′UTR are likely also conserved.

The *Pabpn1* 3′UTR contains multiple predicted *cis*-regulatory elements, including two conserved cleavage/polyadenylation sites (PAS) (22) (Figure 3A). PAS utilization specifies where cleavage and polyadenylation occur which determines 3′ end formation (53–55). If a transcript contains multiple PAS sites, the PAS utilized defines 3′UTR length and potentially inclusion or exclusion of regulatory elements with possible downstream effects on post-transcriptional regulation.

The predominant *Pabpn1* mRNA variant utilizes the distal PAS in all murine tissues examined *in vivo* with the exception of testis (22) To investigate whether PAS usage changes in C2C12 myotubes relative to C2C12 myoblasts, we conducted qRT-PCR using primers that amplify either the coding DNA sequence (CDS) or the distal region of the *Pabpn1* transcript downstream of PASI (Figure 3B). We found no significant change in the ratio of *Pabpn1* alternative PAS utilization in C2C12 myoblasts compared to C2C12 myotubes (Figure 3C), indicating that changes in inclusion or exclusion of regulatory elements does not likely drive differential regulation of *Pabpn1* stability between these cell types. To further investigate *Pabpn1* mRNA variants in C2C12 myoblasts and myotubes, we conducted northern blotting using a radiolabeled *Pabpn1* probe designed to detect *Pabpn1* transcripts generated from use of either PAS. Northern blotting confirmed our qRT-PCR analysis (Figure 1E) showing a decrease in steady-state *Pabpn1* mRNA levels in C2C12 myotubes relative to C2C12 myoblasts (Figure 3D and E). Importantly, these data also demonstrate that the distal PAS is predominantly utilized in both C2C12 myoblasts and C2C12 myotubes (Figure 3D), showing that shifts in alternative polyadenylation do not underlie cell type-specific *Pabpn1* regulation for C2C12 myoblasts or myotubes.

The AU-rich element binding protein HuR interacts with the *Pabpn1* 3′UTR *in vitro*

As the long *Pabpn1* 3′UTR is the predominant variant in C2C12 myotubes, we analyzed predicted *cis*-regulatory elements within this 3′UTR. In this analysis we identified multiple putative AU-rich elements (AREs) (Figure 3A, Supplementary Figure S4A). AREs are present in a subset of transcripts, many which are unstable and require precise control of gene expression (52). RNA binding proteins that recognize AREs can stabilize or destabilize the target transcript by blocking or recruiting RNA degradation machinery (52).

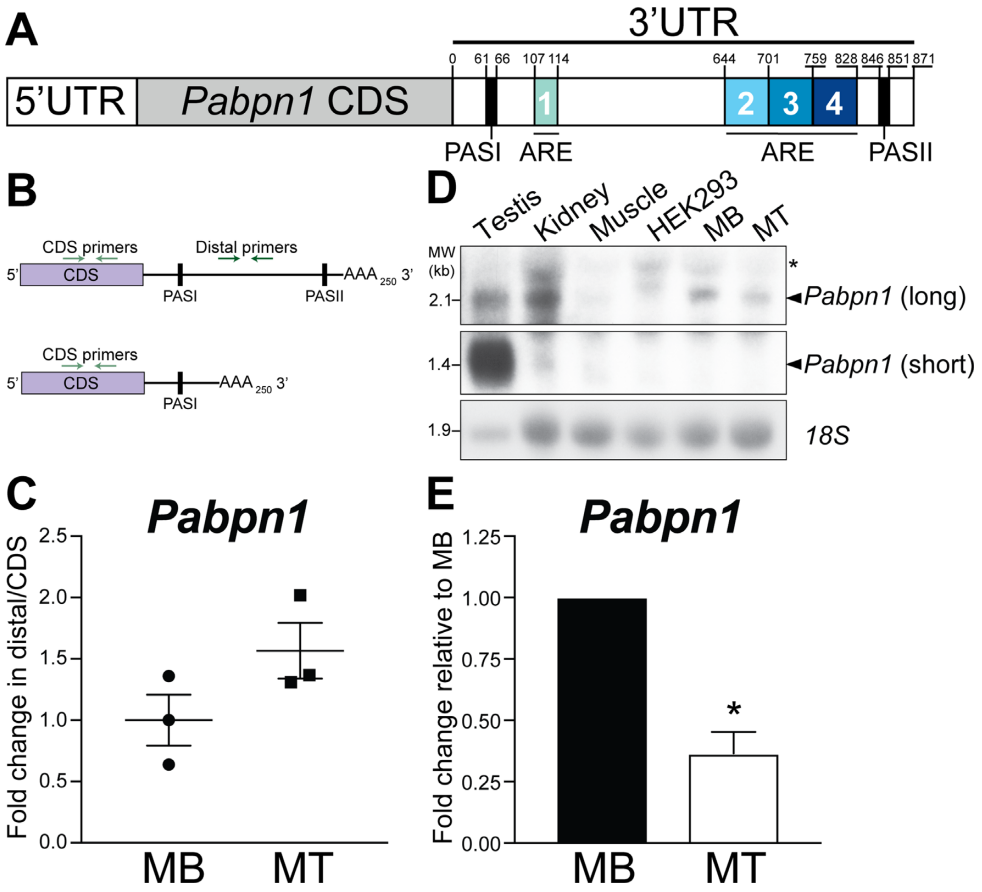

Figure 3. The long *Pabpn1* 3′UTR contains putative conserved *cis*-regulatory elements. (**A**) Schematic of the *Pabpn1* transcript including a 5′ untranslated region (5′UTR), the coding DNA sequence (*Pabpn1* CDS), which encodes the PABPN1 open reading frame, and a 3′ untranslated region (3′UTR) which contains two polyadenylation signals (PASI, PASII) and multiple putative AU-rich elements (ARE1, ARE2, ARE3, ARE4). (**B**) Schematic of qRT-PCR strategy using primers that recognize the coding DNA sequence (CDS primers) and distal (distal primers) regions to determine which polyadenylation site (PASI or PASII) is utilized in C2C12 myoblasts (MB) and C2C12 myotubes (MT). (**C**) qRT-PCR was used to quantify *Pabpn1* levels using primers that recognize the *Pabpn1* CDS or the distal *Pabpn1* 3′UTR. The levels of distal 3′UTR-containing transcripts is calculated relative to CDS-containing transcripts and normalized to *Gapdh.* As described in Materials and Methods, these data are presented as fold change relative to C2C12 myoblasts, for which the average value was set to 1.0. Data are mean ± SEM of $n = 3$ samples per cell type. (**D**) Representative northern blot using a radiolabeled probe recognizing both short (1.4 kb) and long (2.1kb) forms of the *Pabpn1* transcript, corresponding to PASI and PASII utilization (22), respectively, assessing PAS usage in multiple mouse tissues and cell lines including C2C12 myoblasts (MB) and C2C12 myotubes (MT) that have been differentiated for 10 days. Because testis tissue contains high levels of predominantly short *Pabpn1* transcript, this sample was underloaded to avoid strong signal. The *18S* (1.9 kb) rRNA serves as a loading control. Data are representative of $n = 4$ independent biological replicates for C2C12 myotubes and $n = 4$ technical replicates for C2C12 myoblasts. (**E**) Quantification of *Pabpn1* transcript levels from four independent northern blots of RNA prepared from C2C12 myoblasts (MB) and C2C12 myotubes (MT) was performed as described in Materials and Methods. Data were normalized to *18S* rRNA as the loading control and are presented as fold change in *Pabpn1* transcript levels relative to myoblast, which was set to 1.0. Data are mean ± SEM of $n = 4$ ($^*P < 0.05$).

The *Pabpn1* 3′UTR contains several predicted ARE motifs including a single Class I ARE (56) present downstream of the first PAS, denoted as ARE1, and three Class III (56,57) U-rich tracts that are located between PAS I and PAS II (Figure 3A), which we have designated ARE2, ARE3 and ARE4. As one approach to assess whether these predicted AREs are functional, we examined the genomic sequence conservation of these putative AREs (Supplementary Figure S4B). We determined that these four AREs, including A and T-rich tracts encoding A and U in the mRNA, are highly conserved in *Homo sapiens, Bos taurus*, and *Mus musculus* (Supplementary Figure S4B). Thus, these putative AREs could be important for *Pabpn1* regulation. To further dissect whether these putative AREs function as *cis*-regulatory elements in C2C12 myotubes, we transfected C2C12 myotubes with firefly luciferase reporters encoding the murine *Pabpn1* 3′UTR with a deleted PAS1 (ΔPASI) to ensure that a single polyadenylated product is generated, with each reporter containing a single disrupted ARE. To determine if ARE1 is a functional element in C2C12 myotubes, we generated a mutated luciferase reporter where thymines were mutated to guanines (38,39), disrupting the ARE. Because AREs 2, 3 and 4 are ∼60 nucleotides and thus are much longer than the 8 nucleotide ARE1, we generated individual deletion luciferase reporters for AREs 2, 3 and 4. We used these mutated and deleted reporters to determine if disrupting any of these regions in the *Pabpn1* 3′UTR affects expression. ARE1 mutant (Supplementary Figure S3B) does not significantly change luciferase activity relative to control. Similarly, ARE2 deleted (Supplementary Figure S3C) does not significantly change luciferase activity relative to control.

However, ARE3 deleted (Supplementary Figure S3D) significantly increases luciferase activity ∼25% relative to control. Furthermore, ARE4 deleted (Supplementary Figure S3E) significantly increases luciferase activity ∼15% relative to control. Together, these data suggest that ARE3 and ARE4 within the *Pabpn1* 3′UTR function as *cis*-regulatory elements that can negatively regulate expression in C2C12 myotubes.

RNA binding proteins can recognize and bind AREs to regulate mRNA fate. To identify proteins that interact with the *Pabpn1* 3′UTR perhaps through ARE3 or ARE4, we mined available transcriptome-wide cross-linking and immunoprecipitation (CLIP-seq) datasets investigating RNA binding proteins known to bind AREs that are important for regulating muscle biology (58). In these transcriptome-wide studies, the ARE binding protein Human antigen R (HuR) (59) immunoprecipitates the *Pabpn1* transcript in human cervical cancer cells (HeLa) (41) and human embryonic kidney cells (HEK293) (40). Results from these two independent studies identify several HuR binding sites within the *PABPN1* 3′UTR with a single consensus HuR-binding region within the *PABPN1* ARE4 motif (Figure 3A, Supplementary Figure S4B). As differences in HuR binding sites between these cell types could be due to both technical and biological differences, identification of a single consensus binding site within ARE4 of the *PABPN1* 3′UTR gives strong rationale for focusing our studies in muscle on this single consensus HuR binding site.

While HuR canonically stabilizes target transcripts (60) and positively regulates many transcripts in C2C12 myoblasts (61), HuR can also negatively regulate a subset of transcripts through recruitment of degradation factors to specific target mRNAs (61,62). To investigate the potential roles that HuR may play in regulating *Pabpn1* expression in C2C12 myotubes, we tested whether HuR interacts with the *Pabpn1* transcript in lysate prepared from C2C12 myotubes. We performed RNA immunoprecipitation (RIP) followed by qRT-PCR on C2C12 myotube lyate. As expected, HuR is detected in the immunoprecipitated sample but not in the IgG control (Figure 4A). As shown in Figure 4B, the *Pabpn1* transcript is significantly enriched relative to *Gapdh* with HuR immunoprecipitation.

To investigate whether HuR interacts with the *Pabpn1* transcript via the 3′UTR in C2C12 myotube lysate, we utilized a biochemical biotin RNA affinity purification assay. Specifically, we incubated an *in vitro* transcribed biotinylated *Pabpn1* 3′UTR RNA (Supplementary Figure S5) with C2C12 myotube lysate. After isolating biotinylated RNAs and interacting proteins through binding to streptavidin beads, we immunoblotted for candidate RNA binding proteins including HuR. We analyzed two additional RNA binding proteins, the KH-type splicing regulatory protein (KSRP), which targets ARE-containing transcripts for degradation (63) and co-regulates target transcripts with HuR in C2C12 myoblasts (61) and the CUG triplet repeat RNA binding protein (CUGBP1), an RNA binding protein reported to target AREs (64,65) and immunoprecipitates *Pabpn1* mRNA in C2C12 myoblasts (66). Results from this biochemical assay demonstrate that HuR interacts with the *Pabpn1* 3′UTR but not the control *GAPDH* 3′UTR in C2C12 myotube lysate. However, CUGBP1 and KSRP do not interact with either the *Pabpn1* or *GAPDH* 3′UTR in this biochemical assay (Figure 4C). Overall, these data demonstrate that HuR interacts with the *Pabpn1* transcript in C2C12 myotubes, and that HuR interacts with the *Pabpn1* 3′UTR in this biochemical assay.

HuR interacts with a specific region within the *Pabpn1* 3′UTR

As previously described, available HuR CLIP-seq datasets (40,41) show an overlapping HuR CLIP site corresponding with ARE4 in the *Pabpn1* 3′UTR (Figure 5A), an ARE that acts as a *cis*-regulatory element that negatively regulates expression in C2C12 myotubes. To determine if this site contributes to HuR interaction with the *Pabpn1* 3′UTR in C2C12 myotubes, we exploited the biotin RNA affinity purification assay. We incubated C2C12 myotube lysate with two biotinylated *Pabpn1* 3′UTR RNAs *in vitro* transcribed from firefly luciferase constructs: a control 3′UTR with a deleted PAS I (ΔPAS I) and intact ARE4, and an ARE4 mutant RNA (ARE4 mutant) with deleted PAS I and an ARE 4 with thymine-to-guanine mutations disrupting the ARE (38,39) within the HuR CLIP site (Figure 5B, Supplementary Figure S6). We then purified biotinylated RNA and interacting proteins using streptavidin beads and immunoblotted for HuR to determine if ARE4 mutant affects HuR interaction with the *Pabpn1* 3′UTR in this biochemical assay. As shown in Figure 5C and D, there is an ∼60% reduction in HuR protein interaction with the ARE4 mutant *Pabpn1* 3′UTR relative to the control *Pabpn1* 3′UTR. This significant reduction in HuR interaction demonstrates that ARE4, previously shown to bind HuR in HeLa (41) and HEK293 (40) cells, mediates HuR interaction with the *Pabpn1* 3′UTR in C2C12 myotube lysate *in vitro*.

To further assess whether ARE4, which interacts with HuR in C2C12 myotubes, is a *cis*-regulatory element that negatively regulates *Pabpn1* expression in these cells, we conducted luciferase assays in C2C12 myotubes using a reporter with specific mutations disrupting the HuR CLIP site termed ARE4 mutant. We compared relative luciferase activity between two reporters with the *Pabpn1* 3′UTR downstream of firefly luciferase: a control reporter with a deleted PASI, and an ARE4 mutant reporter with a deleted PASI and mutations disrupting the HuR CLIP site in ARE4 (ARE4 mutant, Figure 5B). We deleted PASI to ensure that a single polyadenylated product is generated. As shown in Figure 5E, luciferase activity increases ∼50% with ARE4 mutant relative to control, demonstrating that the region within ARE4 that interacts with HuR negatively regulates expression from the *Pabpn1* 3′UTR in C2C12 myotubes. Overall, these data show that HuR interacts with ARE4 in the *Pabpn1* 3′UTR, and this *cis* element negatively regulates *Pabpn1* expression in C2C12 myotubes.

HuR negatively regulates *Pabpn1* at the RNA and protein levels

To examine the role of HuR in regulating endogenous *Pabpn1* transcript levels, we employed siRNA-mediated depletion of *HuR* in C2C12 myotubes. As previous reports demonstrate that HuR depletion affects C2C12 differentiation (61), we knocked down *HuR* on differentiation day 3

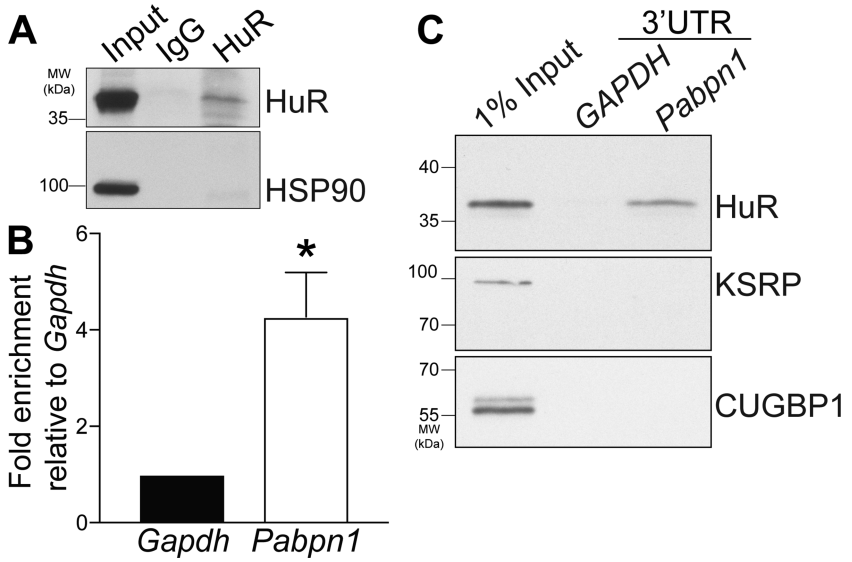

Figure 4. HuR interacts with the *Pabpn1* 3′UTR in C2C12 myotubes. (**A**) Lysates from C2C12 myotubes were immunoprecipitated with α-HuR or control IgG antibody. Immunoblotting was used to detect HuR and the Input sample is also shown. HSP90 is a negative control to show that HuR immunoprecipitation does not purify non-specific proteins. (**B**) HuR-transcript interactions were assessed by RNA immunoprecipitation using qRT-PCR and primers recognizing the *Pabpn1* and *Gapdh* transcripts. Transcript levels are normalized to input and IgG negative control samples. Data are presented as fold enrichment relative to *Gapdh* enrichment for each sample. Data are mean ± SEM of $n = 6$ independent experiments (*$P < 0.05$). (**C**) Biotinylated *GAPDH* and *Pabpn1* 3′UTR RNAs were incubated in C2C12 myotube lysate and the biotinylated RNA along with associated proteins was purified on streptavidin beads. Purified proteins were detected by immunoblotting bound fractions with α-HuR, α-KSRP, and α-CUGBP1 antibodies. The 1% Input lane shows that candidate proteins are present in total C2C12 myotube lysate. Data are representative of $n = 3$ independent experiments.

to ensure that early differentiation stages are not affected. To identify an siRNA that knocks down *HuR* with high efficiency, we tested three independent siRNAs targeting the *HuR* transcript (Supplementary Figure S7A). We determined that siRNA HuR#3 reduces HuR protein levels ∼90% (Supplementary Figure S7A and D), whereas siRNAs HuR#1 and HuR#2 knock down *HuR* less efficiently (Supplementary Figure S7A–C). Therefore, we employed siRNA HuR#3 for our primary analyses.

We confirmed that *HuR* knockdown with siRNA at this stage of C2C12 differentiation does not significantly affect the degree of C2C12 differentiation attained relative to control knockdown by immunoblotting for the late differentiation marker eMyHC (Supplementary Figure S7E) and analyzing cell morphology. We then tested whether PABPN1 protein levels are affected by *HuR* depletion in C2C12 myotubes. As shown in Figure 6A and B, there is a significant increase in PABPN1 protein levels with *HuR* knockdown relative to control. We observe a similar trend towards higher PABPN1 protein levels using two independent siRNAs (Supplementary Figure S7F and G) demonstrating that the change in PABPN1 levels is not due to off target effects of siRNA.

To determine whether this HuR-mediated PABPN1 regulation occurs at the RNA or protein level, we assessed whether steady-state *Pabpn1* mRNA levels also change with HuR depletion. Similar to previous reports (67), we determined that HuR depletion does not affect *Gapdh* transcript levels in C2C12 myotubes, demonstrating that *Gapdh* is an appropriate normalizer for this experiment (Supplementary Figure S7H). Steady-state *Pabpn1* mRNA levels significantly increase ∼1.5-fold with HuR knockdown (Figure 6C). Together these data demonstrate that HuR negatively regulates *Pabpn1* at the RNA and protein levels in C2C12 myotubes.

HuR negatively regulates *Pabpn1 in vivo*

To expand these studies to determine if HuR negatively regulates *Pabpn1* expression *in vivo,* we utilized a muscle-specific *HuR* knockout mouse model ($HuR^{\Delta/\Delta}$) (68, Gallouzi *et al.*, unpublished data). In this mouse, loxP sites flank exon 2 of the *HuR* gene and Cre recombinase is expressed under the control of the muscle-specific *MyoD* promoter. Control $HuR^{fl/fl}$ mice are Cre negative and therefore Cre-mediated recombination does not occur and the *HuR* gene is intact. We confirmed that HuR is not detectable in multiple hindlimb muscles including rectus femoris (Figure 7A) and gastrocnemius (Supplementary Figure S8) muscles from $HuR^{\Delta/\Delta}$ mice but is abundant in control ($HuR^{fl/fl}$) muscles. Therefore, this HuR knockout mouse model can be utilized to study HuR-mediated regulation of *Pabpn1* expression in muscle *in vivo.*

We isolated primary myoblasts from hindlimb muscles of $HuR^{fl/fl}$ and $HuR^{\Delta/\Delta}$mice and used qRT-PCR to assess steady-state *Pabpn1* transcript levels. There was no significant difference in steady-state *Pabpn1* transcript levels in $HuR^{\Delta/\Delta}$ myoblasts relative to $HuR^{fl/fl}$ myoblasts (Figure 7D). We also immunoblotted for PABPN1 protein and found no significant difference in PABPN1 protein levels in $HuR^{\Delta/\Delta}$ myoblasts compared to $HuR^{fl/fl}$ myoblasts (Figure 7B,C). These data demonstrate that HuR does not significantly regulate steady-state *Pabpn1* transcript and protein levels in primary myoblasts.

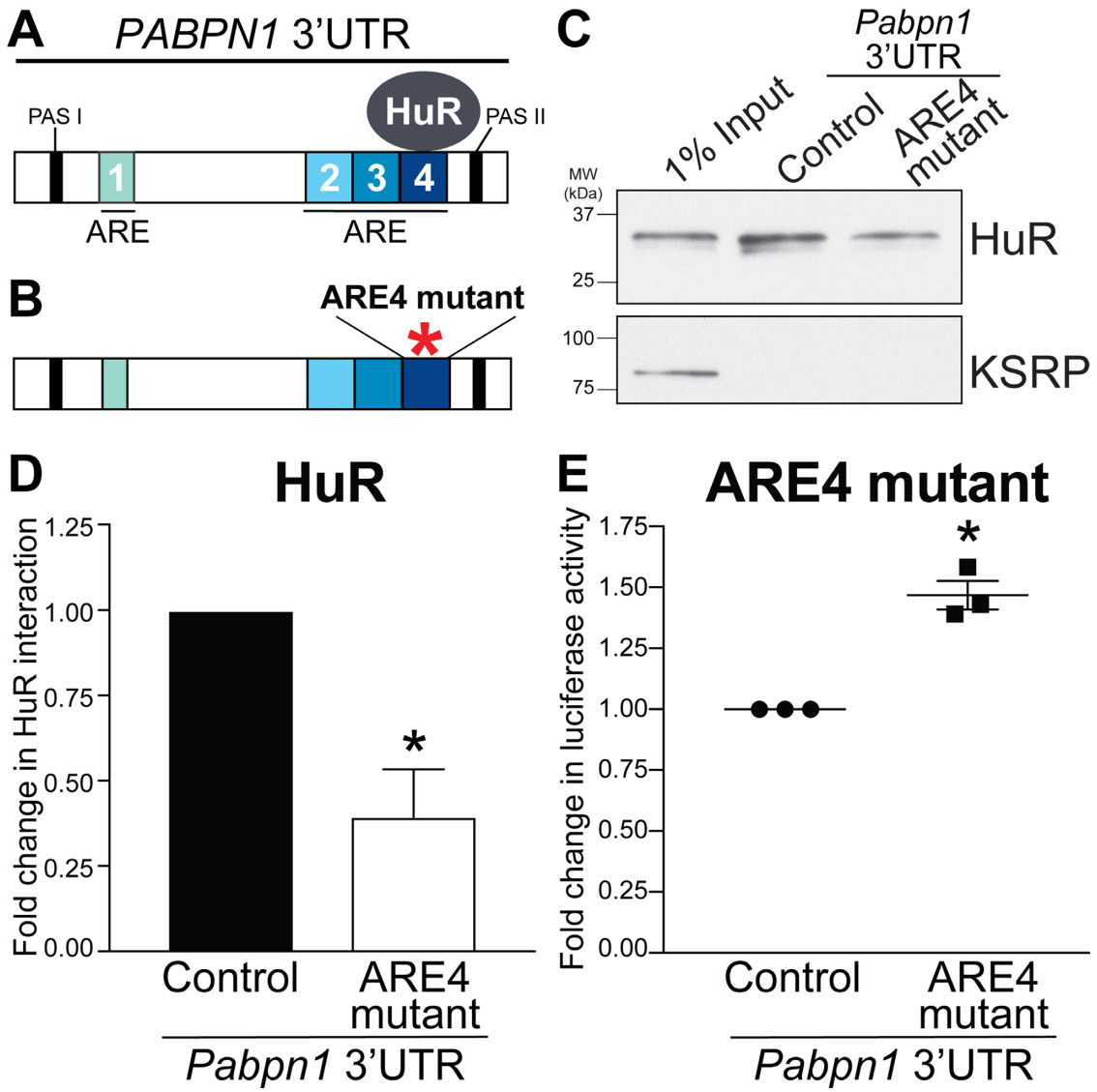

Figure 5. HuR interacts with ARE4, a *cis*-regulatory element that negatively regulates *Pabpn1* expression. (**A**) Schematic illustrating the consensus HuR binding site within the *PABPN1* 3′UTR identified in two transcriptome-wide CLIP-seq studies (40,41). The locations of ARE1, 2, 3 and 4 are indicated as well as PASI and PASII. (**B**) Schematic illustrating the ARE4 mutant sites within the *Pabpn1* 3′UTR. (**C**) Biotinylated Control (deleted PASI) and ARE4 mutant (deleted PASI, mutated HuR CLIP site) *Pabpn1* 3′UTR RNAs were incubated in C2C12 myotube lysate and then purified on streptavidin beads. Immunoblotting with α-HuR and α-KSRP was used to detect purified proteins. The 1% input lane shows that HuR and KSRP are present in total C2C12 myotube lysate. Data represent $n = 3$ independent experiments. (**D**) Quantification of HuR binding to Control and ARE4 mutant *Pabpn1* 3′UTR biotinylated RNAs. Data are normalized to 1% Input and fold change was calculated relative to control, which was set to 1.0. Data are presented as mean ± SEM of $n = 3$ independent experiments (*$P < 0.05$). (**E**) C2C12 myotubes were co-transfected with firefly luciferase reporters with control (deleted PASI) and ARE4 mutant (deleted PASI, mutated HuR CLIP site) *Pabpn1* 3′UTRs and renilla luciferase reporters. Firefly luciferase activity was normalized to renilla luciferase activity as described in Materials and Methods, and the average ratio was set to 1.0 for the control and is presented as mean ± SEM of $n = 3$ independent experiments (*$P < 0.05$).

Our data (Figure 6) suggest that HuR negatively regulates *Pabpn1* in myotubes. To determine whether HuR regulates *Pabpn1* expression in a myotube-specific manner in primary muscle cells, we differentiated primary myoblasts from $HuR^{\Delta/\Delta}$ and $HuR^{fl/fl}$ mice to generate myotubes. As previous reports demonstrate a role for HuR in C2C12 myoblast differentiation (61), we confirmed that these primary $HuR^{\Delta/\Delta}$ myoblasts properly differentiate in the absence of HuR using morphological (Figure 7E) and biochemical (Figure 7F) analyses. In myotubes, we identified a significant ∼1.5 fold increase in *Pabpn1* transcript levels in $HuR^{\Delta/\Delta}$ myotubes relative to $HuR^{fl/fl}$ myotubes (Figure 7G). We also immunoblotted for PABPN1 protein and detected a significant ∼3-fold increase in PABPN1 protein levels in $HuR^{\Delta/\Delta}$ myotubes relative to $HuR^{fl/fl}$ myotubes (Figure 7F and H). Finally, to determine whether HuR could regulate *Pabpn1* expression in muscle tissue, we compared PABPN1 protein levels from $HuR^{fl/fl}$and $HuR^{\Delta/\Delta}$ rectus femoris muscle. As shown in Figure 7I and quantified in Figure 7J, PABPN1 protein levels are significantly higher in $HuR^{\Delta/\Delta}$ muscle compared to $HuR^{fl/fl}$ muscle. These results

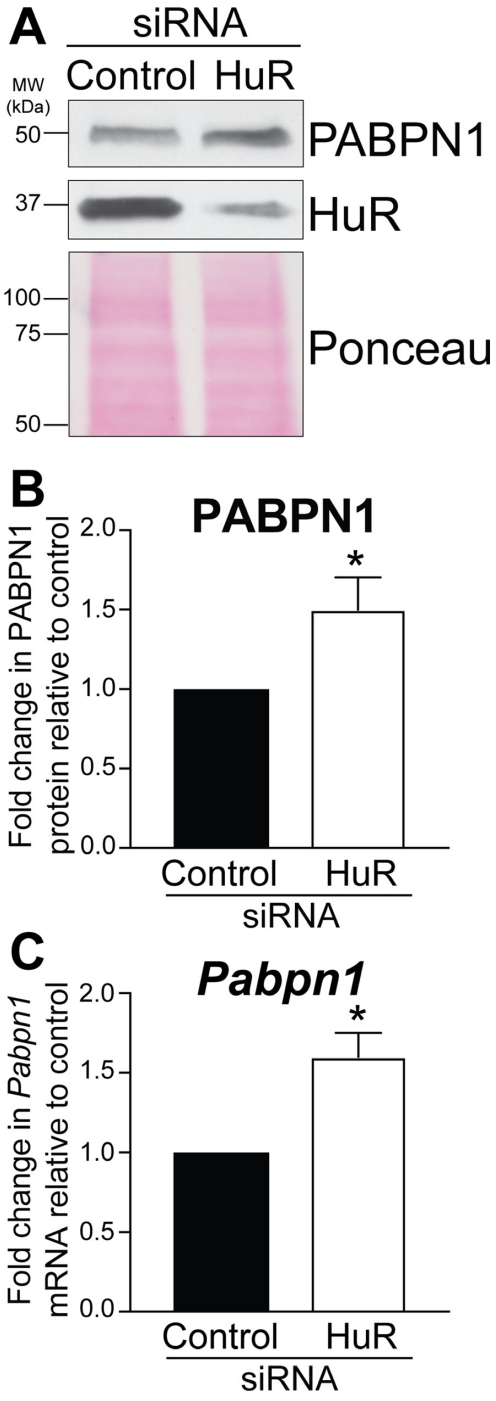

Figure 6. HuR negatively regulates Pabpn1 transcript and protein levels in C2C12 myotubes. C2C12 myotubes were transfected with control siRNA or HuR siRNA (siRNA HuR#3) targeting the *HuR* transcript. (**A**) Control and HuR knockdown C2C12 myotube lysates were immunoblotted with α-PABPN1 and α-HuR antibodies. Ponceau stain serves as a loading control. The immunoblot shown is representative of $n = 4$ independent experiments. (**B**) Quantification of α-PABPN1 immunoblot from control and HuR knockdown samples. Data are presented as fold change in PABPN1 relative to control knockdown, which was set to 1.0. Data are presented ± SEM of $n = 4$ independent experiments (*$P < 0.05$). (**C**) qRT-PCR was used to assess the steady-state levels of the *Pabpn1* transcript from control and HuR knockdown samples. *Pabpn1* levels are normalized to *Gapdh* and presented as fold change relative to control siRNA samples. Data are presented as ± SEM of $n = 4$ independent experiments (*$P < 0.05$).

validate our *in vitro* studies and demonstrate that HuR negatively regulates *Pabpn1* expression *in vivo.*

To begin to interrogate the mechanisms underlying this HuR-mediated *Pabpn1* regulation in myotubes, we conducted luciferase assays assessing whether HuR negatively regulates *Pabpn1* expression through ARE4. We conducted luciferase assays in primary $HuR^{fl/fl}$and $HuR^{\Delta/\Delta}$ myotubes using the same reporters assayed in Figure 5D including a luciferase reporter encoding a control *Pabpn1* 3′UTR and an ARE4 mutant luciferase reporter which has specific mutations disrupting the HuR CLIP site within ARE4 (Figure 7K). Similar to observations presented in Figure 5D, we detect a significant ∼50% increase in luciferase activity in $HuR^{fl/fl}$myotubes when ARE4 is mutated relative to control (Figure 7L). However, when $HuR^{\Delta/\Delta}$ myotubes are transfected with ARE4 mutant luciferase reporters, we observe no significant difference in luciferase activity relative to control (Figure 7L). Although we observed a modest increase in luciferase activity when $HuR^{\Delta/\Delta}$ myotubes are transfected with ARE4 mutant luciferase reporters, this increase is not significant perhaps due to experimental variability observed when $HuR^{\Delta/\Delta}$ myotubes are transfected with control reporters. Together, these data demonstrate that HuR-mediated *Pabpn1* regulation depends on ARE4 within the *Pabpn1* 3′UTR in primary myotubes.

HuR is more cytoplasmic in C2C12 myotubes than C2C12 myoblasts

To further dissect the mechanisms underlying HuR-mediated *Pabpn1* regulation in mature muscle, we used immunoblotting to assess whether HuR protein levels change in C2C12 myoblasts compared to myotubes. There was no significant change in total HuR protein levels in C2C12 myotubes relative to C2C12 myoblasts (Figure 8A and B). However, HuR shuttles between the nucleus and cytoplasm (69) raising the possibility that differential localization of HuR could confer myotube-specific regulation of *Pabpn1* expression. To determine whether a change in the steady-state localization of HuR correlates with differential regulation of *Pabpn1* expression in myoblasts and myotubes, we assessed the subcellular localization of HuR in these cells using biochemical fractionation (Figure 8C). As expected (30,70), HuR is primarily nuclear in both C2C12 myoblasts and C2C12 myotubes (Figure 8C). However, there is an increase in the level of cytoplasmic HuR in C2C12 myotubes compared to C2C12 myoblasts (Figure 8C), consistent with previous observations (67,71,72). As the cytoplasm of myotubes contain high levels of muscle-specific proteins (e.g. embryonic Myosin Heavy Chain, eMyHC, as shown in Figure 1C), we assessed the amount of cytoplasmic HuR in C2C12 myotubes relative to another cytoplasmic (73,74), non-muscle-specific protein GAPDH (Figure 8C). Using this metric, there is a significant increase in cytoplasmic HuR in C2C12 myotubes compared to C2C12 myoblasts (Figure 8D). These data suggest that interaction of HuR with the *Pabpn1* transcript in the cytoplasm could contribute to HuR-mediated *Pabpn1* regulation specifically in mature muscle.

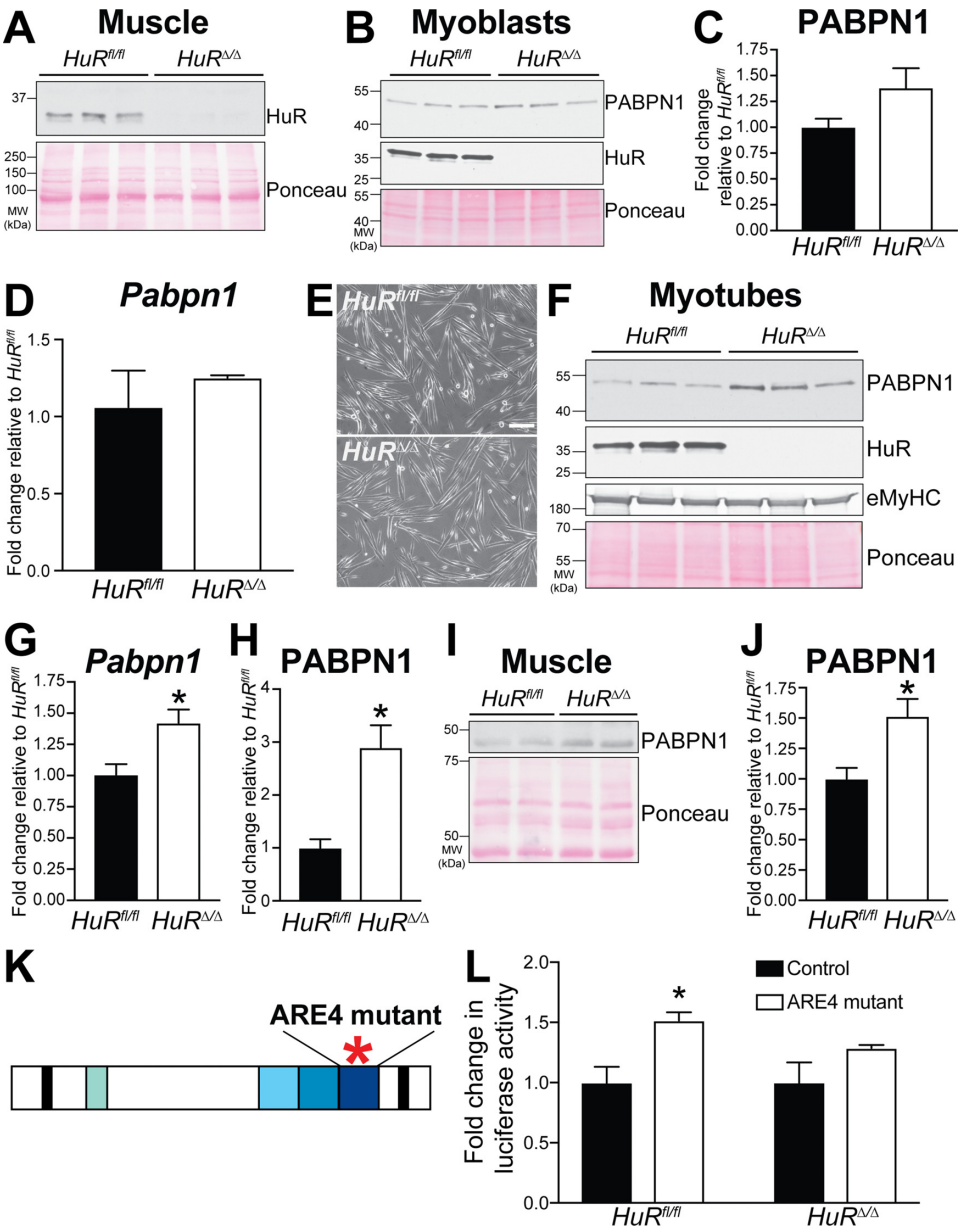

Figure 7. HuR negatively regulates *Pabpn1* transcript and protein levels specifically in mature muscle *in vitro* and *in vivo.* (**A**) Immunoblot using α-HuR antibody to analyze HuR protein levels in rectus femoris muscle from 3-month-old male control ($HuR^{fl/fl}$) and HuR knockout ($HuR^{\Delta/\Delta}$) mice. For each genotype, samples were prepared in parallel from three independent mice. Ponceau stain serves as a loading control. (**B**) Lysate from primary myoblasts isolated from $HuR^{fl/fl}$ and $HuR^{\Delta/\Delta}$ mice was immunoblotted with α-PABPN1 and α-HuR antibodies. Primary myoblasts were prepared and analyzed in biological triplicate per genotype. Ponceau stain serves as a loading control. (**C**) Quantification of PABPN1 protein levels in $HuR^{fl/fl}$ and $HuR^{\Delta/\Delta}$ primary myoblasts. Data are presented as fold change in PABPN1 levels relative to the mean levels detected in $HuR^{fl/fl}$ myoblasts and plotted as ± SEM of $n = 3$ samples. (**D**) qRT-PCR was used to assess steady-state *Pabpn1* transcript levels in $HuR^{fl/fl}$ and $HuR^{\Delta/\Delta}$ primary myoblasts. As described in Materials and Methods, data are normalized to *Gapdh* and are presented as mean fold change relative to mean *Pabpn1* transcript levels detected in $HuR^{fl/fl}$ myoblasts as ± SEM of $n = 3$ samples. (**E**) Representative images of primary $HuR^{fl/fl}$ and $HuR^{\Delta/\Delta}$ myotubes. Bar = 100μm. (**F**) Lysate from three biological replicates of $HuR^{fl/fl}$ and $HuR^{\Delta/\Delta}$ primary myotubes was immunoblotted with α-PABPN1, α-HuR, and α-eMyHC antibodies. Ponceau stain serves as a loading control. Data are $n = 3$ samples. (**G**) qRT-PCR was used to assess steady-state *Pabpn1* transcript levels in $HuR^{fl/fl}$ and $HuR^{\Delta/\Delta}$ primary myotubes. *Pabpn1* transcript levels are normalized to *Gapdh* and fold change is calculated relative to the mean, normalized *Pabpn1* levels observed in $HuR^{fl/fl}$ primary myotubes. Data are presented as mean ± SEM of $n = 3$ samples ($^*P < 0.05$). (**H**) Quantification of immunoblot (**F**) assessing PABPN1 protein levels in $HuR^{fl/fl}$ and $HuR^{\Delta/\Delta}$ primary myotubes. PABPN1 levels are normalized to Ponceau stain and presented as fold change compared to the average levels observed in $HuR^{fl/fl}$ primary myotubes, which was set to 1.0. Data are presented for mean ± SEM of $n = 3$ samples ($^*P < 0.05$). (**I**) Lysates from rectus femoris muscle tissue from 3-month-old male $HuR^{fl/fl}$ and $HuR^{\Delta/\Delta}$ mice was immunoblotted with α-PABPN1 to determine PABPN1 protein levels. Results are presented for biological duplicates. Ponceau stain serves as a loading control. (**J**) Quantification of immunoblot analyzing PABPN1 levels in $HuR^{fl/fl}$ and $HuR^{\Delta/\Delta}$ rectus femoris muscle tissue. Data are presented as fold change relative to the average for the $HuR^{fl/fl}$ sample, which was set to 1.0. Data shown represent the mean ± SEM of $n = 3$ samples ($^*P < 0.05$). (**K**) Schematic of ARE4 mutant *Pabpn1* 3′UTR firefly luciferase reporter. (**L**) Primary $HuR^{fl/fl}$ and $HuR^{\Delta/\Delta}$ myotubes were co-transfected with firefly luciferase reporters with control (deleted PASI) or ARE4 mutant (deleted PASI, mutated ARE4) *Pabpn1* 3′UTRs and renilla luciferase reporters. Firefly luciferase activity was normalized to renilla luciferase activity as described in Materials and Methods, and the average ratio was set to 1.0 for the control and is presented as mean ± SEM of $n = 3$ independent experiments ($^*P<0.05$).

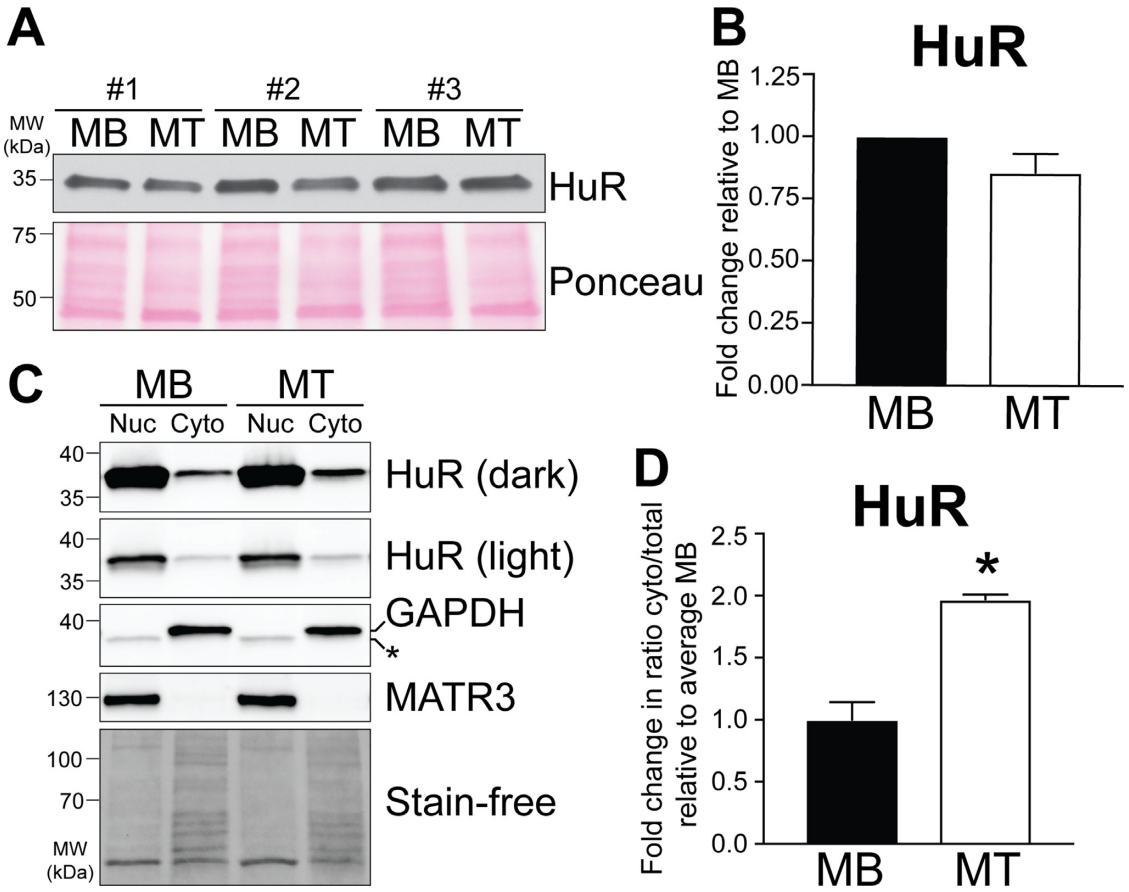

Figure 8. HuR localization is more cytoplasmic in C2C12 myotubes than C2C12 myoblasts. (**A**) C2C12 myoblast (MB) and C2C12 myotube (MT) lysates were immunoblotted with α-HuR antibody to determine HuR protein levels in these cells. For this experiment the C2C12 myoblast sample analyzed was then differentiated into the myotube sample analyzed for each biological replicate (#1, #2 and #3). Ponceau stain serves as a loading control. (**B**) Quantification of the immunoblot shown in (**A**). HuR levels are presented as fold change relative to mean levels detected in C2C12 myoblasts (MB), which was set to 1.0. Data are presented as mean ± SEM of $n = 3$ samples. (**C**) Representative immunoblot showing cellular fractionation performed on C2C12 myoblasts (MB) and C2C12 myotubes (MT). Two exposures are shown for the HuR blot (dark and light) to ensure that both cytoplasmic signal (dark) and nuclear signal (light) are shown in the linear range. Nuclear and cytoplasmic fractions were analyzed by immunoblotting with α-HuR. Matrin3 (α-MATR3) is a control nuclear protein, and α-GAPDH is a control cytoplasmic protein. Stain-free serves as a loading control. (**D**) Quantification of subcellular HuR localization in C2C12 myoblasts (MB) and C2C12 myotubes (MT). Data were normalized to their respective subcellular protein controls (MATR3 for the nuclear fraction and GAPDH for the cytoplasmic fraction). The ratio of cytoplasmic/total protein detected was calculated and is presented as fold change relative to the mean ratio calculated for C2C12 myoblasts. Data are presented as mean ± SEM of $n = 3$ biological replicates (*$P < 0.05$).

DISCUSSION

This study takes a first step in providing insight into how expression of the *Pabpn1* gene is regulated in mature muscle. We identify multiple *cis*-regulatory elements in the *Pabpn1* 3′UTR and characterize HuR-mediated *Pabpn1* regulation both *in vitro* and *in vivo*. While we identify HuR as one *trans*-acting factor that regulates expression of *Pabpn1*, our data support a model where HuR is one of multiple regulatory factors that modulate PABPN1 expression in mature muscle.

Our previous work showed that PABPN1 levels are low in mature muscle but not in primary myoblasts and non-muscle tissues (22). Using *in vivo* models to uncover the mechanisms underlying this regulation in muscle tissue would be challenging. We used a mouse cell culture model of mature muscle to identify and define *cis*-regulatory elements and *trans*-acting factors that modulate *Pabpn1* expression. We validated this *in vitro* model of mature muscle, C2C12 myotubes. Aspects of *Pabpn1* gene expression identified *in vivo* (22) are similar in C2C12 myotubes, including reduced *Pabpn1* transcript stability and low steady-state *Pabpn1* transcript and protein levels in C2C12 myotubes relative to myoblasts. Furthermore, our work shows that regulatory mechanisms discovered in this *in vitro* model of mature muscle are conserved *in vivo*. Therefore, this *in vitro* model can be used for future work studying how *cis*- and *trans*-acting factors regulate gene expression in mature muscle.

Previous work identified a 50-fold decrease in steady-state *Pabpn1* transcript levels in mouse muscle tissue compared to primary myoblasts isolated from muscle tissue (22). To begin to uncover the mechanisms that contribute to this muscle tissue-specific *Pabpn1* regulation, we established a tractable system utilizing C2C12 myoblasts and myotubes. This system allows mechanistic experiments to be conducted to interrogate the post-transcriptional mechanisms that could contribute to this muscle tissue-specific

regulation. While we detect a significant decrease in steady-state *Pabpn1* transcript levels in C2C12 myotubes relative to C2C12 myoblasts, the magnitude of this downregulation is substantially less than the 50-fold decrease detected in muscle tissue relative to primary myoblasts (22). Likely this change in magnitude reflects the fact that a C2C12 myotube is not as different from a proliferating C2C12 myoblast as mature muscle tissue is from isolated primary myoblasts. Importantly, we have validated the results obtained in the C2C12 model through *in vivo* studies of mouse muscle that confirm a role for HuR as a negative regulator of PABPN1 expression.

We defined multiple *cis*-regulatory elements in the *Pabpn1* 3′UTR including two functional AU-rich elements (AREs). AREs are present in only ∼8% of mRNAs, and many of these ARE-containing transcripts are short-lived and require precise control of gene expression (52). AREs interact with RNA binding proteins that stabilize or destabilize the target transcript. We investigated whether several candidate ARE binding proteins that play important roles in muscle biology (30,58) interact with the *Pabpn1* 3′UTR. Our results show that the well-characterized ARE-binding protein HuR binds to the *Pabpn1* 3′UTR. Two other candidate ARE-binding proteins, KSRP and CUGBP1, did not bind the *Pabpn1* 3′UTR in a biochemical assay. Our analysis does not preclude the possibility that KSRP and/or CUGBP1 could bind elsewhere in the *Pabpn1* transcript or could regulate *Pabpn1* expression in other cell types. Therefore, we have defined two regulatory elements in the *Pabpn1* 3′UTR and have identified a *trans*-acting factor, HuR, which negatively regulates the *Pabpn1* transcript in mature muscle.

The conventional function of the ubiquitous ARE-binding protein HuR (59) is stabilization of ARE-containing target transcripts by preventing recruitment of RNA degradation machinery (67,71). However, recent reports show that HuR can destabilize specific target transcripts in C2C12 myoblasts (61) and other cell types (62,75,76). Our data demonstrate that ARE3 and ARE4 negatively regulate *Pabpn1* expression in C2C12 myotubes, and that HuR binds specifically to ARE4 in a biochemical assay. Mutation of ARE4 causes a ∼60% decrease in HuR binding to the *Pabpn1* 3′UTR, suggesting that HuR can also bind to other regions within the *Pabpn1* transcript. Furthermore, the ARE4 site is required for HuR-dependent regulation of *Pabpn1* levels. These data are consistent with previous reports demonstrating that HuR crosslinks to four sites within the *Pabpn1* 3′UTR in HEK293 cells (40). However, only one of these crosslinked regions, corresponding to ARE4, was also identified in HuR crosslinking data from HeLa cells (41) indicating that HuR binding sites within the *Pabpn1* 3′UTR are likely cell-type dependent and may be influenced by additional *trans*-acting factors such as microRNAs or other RNA binding proteins.

This study provides insight into the mechanisms that underlie the muscle-specific decrease in *Pabpn1* transcript and protein levels *in vivo*. We show both *in vitro* using C2C12 myotubes and primary myotubes and *in vivo* that HuR negatively regulates *Pabpn1* transcript and protein levels. Importantly, experiments comparing primary myoblasts and myotubes show that this HuR-mediated *Pabpn1* regulation is myotube specific, as steady-state *Pabpn1* transcript and protein levels do not change with HuR depletion in myoblasts. These results suggest that differences must exist in the regulation of *Pabpn1* transcript in myotubes compared to myoblasts.

While we detected no change in total HuR levels when we compared myotubes and myoblasts, we did discover a change in HuR localization that could contribute to myotube-specific regulation of *Pabpn1*. Although the steady-state localization of HuR is predominantly nuclear, HuR shuttles between the nucleus and the cytoplasm (69). Phosphorylation can regulate HuR localization (70), which can affect HuR-mediated regulation of RNA target stability as most properly processed mRNAs are degraded in the cytoplasm (77). Our data show that HuR is primarily nuclear in both C2C12 myoblasts and C2C12 myotubes (30). However, we detect more cytoplasmic HuR in C2C12 myotubes compared to myoblasts, which is consistent with previous reports (72) and could contribute to HuR-mediated *Pabpn1* regulation occurring specifically in mature muscle.

Although we explored a role for HuR in regulating *Pabpn1* mRNA levels, additional cytoplasmic functions for HuR include regulation of translation and interplay with microRNAs (78–81). HuR can both promote and repress translation of target transcripts through binding at the 3′UTR (78) including through binding U-rich tracts in the 3′UTR (79). HuR can also recruit microRNAs to repress translation (80), and reports in C2C12 myoblasts (79) and cancer cells (81) demonstrate that HuR and microRNAs/noncoding RNAs can have antagonistic effects on translation. Furthermore, HuR and microRNA targets commonly overlap in 3′UTRs, suggesting another level of complexity (82). Therefore, the regulatory mechanisms of HuR, including stabilizing/destabilizing transcripts and promoting/repressing translation, are likely influenced by *trans*-acting factors including microRNAs that could interact with the transcript under specific cellular conditions. Additional mechanisms regulating HuR could also be involved, such as HuR cleavage as a mechanism to regulate cytoplasmic HuR accumulation (71). Furthermore, a recent study showed that a circular RNA, *CircPABPN1*, generated from *PABPN1* pre-mRNA binds and sequesters HuR in HeLa cells (83). This study also demonstrated that HuR is a positive regulator of PABPN1 translation in HeLa cells. While we did not directly examine translation in the present study, HuR could play multiple roles in regulating PABPN1 expression. Future work is needed to determine whether *CircPABPN1* is expressed in muscle tissue and cells, and whether *CircPABPN1* functions as a HuR sponge in a similar manner in muscle as observed in HeLa cells and whether the molecular and biological consequences of sequestering HuR could diverge across these cell types. Overall, the mechanism by which HuR negatively regulates *Pabpn1* expression specifically in mature muscle is likely complex involving multiple RNA binding proteins, microRNAs, and could affect *Pabpn1* regulation at both the RNA- and protein-levels.

Together, this work has exploited multiple models to elucidate mechanisms that confer mature-muscle-specific regulation of the *Pabpn1* transcript. Identification of this regulatory mechanism could provide an opportunity to modulate

PABPN1 protein levels perhaps by disrupting HuR recognition of the binding site in ARE4 in the *Pabpn1* 3′UTR. Low PABPN1 protein levels in tissues affected in patients with OPMD could explain why particular muscles are affected in this disease, and exploiting defined regulatory pathways that increase PABPN1 protein levels could be protective for OPMD patients.

SUPPLEMENTARY DATA

Supplementary Data are available at NAR Online.

ACKNOWLEDGEMENTS

This work was supported in part by the Emory Integrated Genomics Core (EIGC), which is subsidized by the Emory University School of Medicine and is one of the Emory Integrated Core Facilities. The content is solely the responsibility of the authors and does not necessarily reflect the official views of the National Institutes of Health.

FUNDING

National Institutes of Health (NIH) [5R01AR061987 to G.K.P., A.H.C., 5F31AR069994 to B.L.P.]; Muscular Dystrophy Association [422006 to A.H.C.]; Canadian Institute for Health Research Operating Grant [MOP-142399 to I.E.G.]. Funding for open access charge: NIH [2R01AR061987].

Conflict of interest statement. None declared.

REFERENCES

1. Kechavarzi,B. and Janga,S.C. (2014) Dissecting the expression landscape of RNA-binding proteins in human cancers. *Genome Biol.*, **15**, R14.
2. Gerstberger,S., Hafner,M. and Tuschl,T. (2014) A census of human RNA-binding proteins. *Nat. Rev. Genet.*, **15**, 829–845.
3. Brais,B., Bouchard,J.P., Xie,Y.G., Rochefort,D.L., Chretien,N., Tome,F.M., Lafreniere,R.G., Rommens,J.M., Uyama,E., Nohira,O. *et al.* (1998) Short GCG expansions in the PABP2 gene cause oculopharyngeal muscular dystrophy. *Nat. Genet.*, **18**, 164–167.
4. Banerjee,A., Apponi,L.H., Pavlath,G.K. and Corbett,A.H. (2013) PABPN1: molecular function and muscle disease. *FEBS J.*, **280**, 4230–4250.
5. Wahle,E. (1991) A novel poly(A)-binding protein acts as a specificity factor in the second phase of messenger RNA polyadenylation. *Cell*, **66**, 759–768.
6. Wahle,E., Lustig,A., Jeno,P. and Maurer,P. (1993) Mammalian poly(A)-binding protein II. Physical properties and binding to polynucleotides. *J. Biol. Chem.*, **268**, 2937–2945.
7. Apponi,L.H., Leung,S.W., Williams,K.R., Valentini,S.R., Corbett,A.H. and Pavlath,G.K. (2010) Loss of nuclear poly(A)-binding protein 1 causes defects in myogenesis and mRNA biogenesis. *Hum. Mol. Genet.*, **19**, 1058–1065.
8. Bresson,S.M., Hunter,O.V., Hunter,A.C. and Conrad,N.K. (2015) Canonical Poly(A) polymerase activity promotes the decay of a wide variety of mammalian nuclear RNAs. *PLos Genet.*, **11**, e1005610.
9. de Klerk,E., Venema,A., Anvar,S.Y., Goeman,J.J., Hu,O., Trollet,C., Dickson,G., den Dunnen,J.T., van der Maarel,S.M., Raz,V. *et al.* (2012) Poly(A) binding protein nuclear 1 levels affect alternative polyadenylation. *Nucleic Acids Res.*, **40**, 9089–9101.
10. Jenal,M., Elkon,R., Loayza-Puch,F., van Haaften,G., Kuhn,U., Menzies,F.M., Oude Vrielink,J.A., Bos,A.J., Drost,J., Rooijers,K. *et al.* (2012) The poly(A)-binding protein nuclear 1 suppresses alternative cleavage and polyadenylation sites. *Cell*, **149**, 538–553.
11. Li,W., You,B., Hoque,M., Zheng,D., Luo,W., Ji,Z., Park,J.Y., Gunderson,S.I., Kalsotra,A., Manley,J.L. *et al.* (2015) Systematic profiling of poly(A)+ transcripts modulated by core 3′ end processing and splicing factors reveals regulatory rules of alternative cleavage and polyadenylation. *PLos Genet.*, **11**, e1005166.
12. Liu,X., Hoque,M., Larochelle,M., Lemay,J.F., Yurko,N., Manley,J.L., Bachand,F. and Tian,B. (2017) Comparative analysis of alternative polyadenylation in S. cerevisiae and S. pombe. *Genome Res.*, **27**, 1685–1695.
13. Vest,K.E., Phillips,B.L., Banerjee,A., Apponi,L.H., Dammer,E.B., Xu,W., Zheng,D., Yu,J., Tian,B., Pavlath,G.K. *et al.* (2017) Novel mouse models of oculopharyngeal muscular dystrophy (OPMD) reveal early onset mitochondrial defects and suggest loss of PABPN1 may contribute to pathology. *Hum. Mol. Genet.*, **26**, 3235–3252.
14. Kuhn,U., Nemeth,A., Meyer,S. and Wahle,E. (2003) The RNA binding domains of the nuclear poly(A)-binding protein. *J. Biol. Chem.*, **278**, 16916–16925.
15. Calado,A., Tome,F.M., Brais,B., Rouleau,G.A., Kuhn,U., Wahle,E. and Carmo-Fonseca,M. (2000) Nuclear inclusions in oculopharyngeal muscular dystrophy consist of poly(A) binding protein 2 aggregates which sequester poly(A) RNA. *Hum. Mol. Genet.*, **9**, 2321–2328.
16. Tome,F.M. and Fardeau,M. (1980) Nuclear inclusions in oculopharyngeal dystrophy. *Acta Neuropathol.*, **49**, 85–87.
17. Davies,J.E., Wang,L., Garcia-Oroz,L., Cook,L.J., Vacher,C., O'Donovan,D.G. and Rubinsztein,D.C. (2005) Doxycycline attenuates and delays toxicity of the oculopharyngeal muscular dystrophy mutation in transgenic mice. *Nat. Med.*, **11**, 672–677.
18. Winter,R., Kuhn,U., Hause,G. and Schwarz,E. (2012) Polyalanine-independent conformational conversion of nuclear poly(A)-binding protein 1 (PABPN1). *J. Biol. Chem.*, **287**, 22662–22671.
19. Berciano,M.T., Villagra,N.T., Ojeda,J.L., Navascues,J., Gomes,A., Lafarga,M. and Carmo-Fonseca,M. (2004) Oculopharyngeal muscular dystrophy-like nuclear inclusions are present in normal magnocellular neurosecretory neurons of the hypothalamus. *Hum. Mol. Genet.*, **13**, 829–838.
20. Villagra,N.T., Bengoechea,R., Vaque,J.P., Llorca,J., Berciano,M.T. and Lafarga,M. (2008) Nuclear compartmentalization and dynamics of the poly(A)-binding protein nuclear 1 (PABPN1) inclusions in supraoptic neurons under physiological and osmotic stress conditions. *Mol. Cell. Neurosci.*, **37**, 622–633.
21. Dion,P., Shanmugam,V., Gaspar,C., Messaed,C., Meijer,I., Toulouse,A., Laganiere,J., Roussel,J., Rochefort,D., Laganiere,S. *et al.* (2005) Transgenic expression of an expanded (GCG)13 repeat PABPN1 leads to weakness and coordination defects in mice. *Neurobiol. Dis.*, **18**, 528–536.
22. Apponi,L.H., Corbett,A.H. and Pavlath,G.K. (2013) Control of mRNA stability contributes to low levels of nuclear poly(A) binding protein 1 (PABPN1) in skeletal muscle. *Skelet Muscle*, **3**, 23.
23. Kusters,B., van Hoeve,B.J., Schelhaas,H.J., Ter Laak,H., van Engelen,B.G. and Lammens,M. (2009) TDP-43 accumulation is common in myopathies with rimmed vacuoles. *Acta Neuropathol.*, **117**, 209–211.
24. Fan,X., Messaed,C., Dion,P., Laganiere,J., Brais,B., Karpati,G. and Rouleau,G.A. (2003) HnRNP A1 and A/B interaction with PABPN1 in oculopharyngeal muscular dystrophy. *Can. J. Neurol. Sci.*, **30**, 244–251.
25. Klein,P., Oloko,M., Roth,F., Montel,V., Malerba,A., Jarmin,S., Gidaro,T., Popplewell,L., Perie,S., Lacau St Guily,J. *et al.* (2016) Nuclear poly(A)-binding protein aggregates misplace a pre-mRNA outside of SC35 speckle causing its abnormal splicing. *Nucleic Acids Res.*, **44**, 10929–10945.
26. Simionescu-Bankston,A., Leoni,G., Wang,Y., Pham,P.P., Ramalingam,A., DuHadaway,J.B., Faundez,V., Nusrat,A., Prendergast,G.C. and Pavlath,G.K. (2013) The N-BAR domain protein, Bin3, regulates Rac1- and Cdc42-dependent processes in myogenesis. *Dev. Biol.*, **382**, 160–171.
27. Gallouzi,I.E., Brennan,C.M., Stenberg,M.G., Swanson,M.S., Eversole,A., Maizels,N. and Steitz,J.A. (2000) HuR binding to cytoplasmic mRNA is perturbed by heat shock. *Proc. Natl. Acad. Sci. U.S.A.*, **97**, 3073–3078.

28. Horsley,V., Jansen,K.M., Mills,S.T. and Pavlath,G.K. (2003) IL-4 acts as a myoblast recruitment factor during mammalian muscle growth. *Cell*, **113**, 483–494.
29. Livak,K.J. and Schmittgen,T.D. (2001) Analysis of relative gene expression data using real-time quantitative PCR and the 2(-Delta Delta C(T)) Method. *Methods*, **25**, 402–408.
30. Figueroa,A., Cuadrado,A., Fan,J., Atasoy,U., Muscat,G.E., Munoz-Canoves,P., Gorospe,M. and Munoz,A. (2003) Role of HuR in skeletal myogenesis through coordinate regulation of muscle differentiation genes. *Mol. Cell. Biol.*, **23**, 4991–5004.
31. Abernathy,E., Gilbertson,S., Alla,R. and Glaunsinger,B. (2015) Viral nucleases induce an mRNA Degradation-Transcription feedback loop in mammalian cells. *Cell Host Microbe*, **18**, 243–253.
32. Conrad,N.K., Mili,S., Marshall,E.L., Shu,M.D. and Steitz,J.A. (2006) Identification of a rapid mammalian deadenylation-dependent decay pathway and its inhibition by a viral RNA element. *Mol. Cell*, **24**, 943–953.
33. Anantharaman,A., Gholamalamdari,O., Khan,A., Yoon,J.H., Jantsch,M.F., Hartner,J.C., Gorospe,M., Prasanth,S.G. and Prasanth,K.V. (2017) RNA-editing enzymes ADAR1 and ADAR2 coordinately regulate the editing and expression of Ctn RNA. *FEBS Lett.*, **591**, 2890–2904.
34. Kent,W.J., Sugnet,C.W., Furey,T.S., Roskin,K.M., Pringle,T.H., Zahler,A.M. and Haussler,D. (2002) The human genome browser at UCSC. *Genome Res.*, **12**, 996–1006.
35. Mouse Genome Sequencing Consortium, Waterston,R.H., Lindblad-Toh,K., Birney,E., Rogers,J., Abril,J.F, Agarwal,P., Agarwala,R., Ainscough,R., Alexandersson,M. *et al.* (2002) Initial sequencing and comparative analysis of the mouse genome. *Nature*, **420**, 520–562.
36. Zimin,A.V., Delcher,A.L., Florea,L., Kelley,D.R., Schatz,M.C., Puiu,D., Hanrahan,F., Pertea,G., Van Tassell,C.P., Sonstegard,T.S. *et al.* (2009) A whole-genome assembly of the domestic cow, Bos taurus. *Genome Biol.*, **10**, R42.
37. Lau,A.G., Irier,H.A., Gu,J., Tian,D., Ku,L., Liu,G., Xia,M., Fritsch,B., Zheng,J.Q., Dingledine,R. *et al.* (2010) Distinct 3′UTRs differentially regulate activity-dependent translation of brain-derived neurotrophic factor (BDNF). *Proc. Natl. Acad. Sci. U.S.A.*, **107**, 15945–15950.
38. Nagaoka,K., Suzuki,T., Kawano,T., Imakawa,K. and Sakai,S. (2006) Stability of casein mRNA is ensured by structural interactions between the 3′-untranslated region and poly(A) tail via the HuR and poly(A)-binding protein complex. *Biochim. Biophys. Acta*, **1759**, 132–140.
39. Chen,C.Y. and Shyu,A.B. (1995) AU-rich elements: characterization and importance in mRNA degradation. *Trends Biochem. Sci.*, **20**, 465–470.
40. Mukherjee,N., Corcoran,D.L., Nusbaum,J.D., Reid,D.W., Georgiev,S., Hafner,M., Ascano,M. Jr., Tuschl,T., Ohler,U. and Keene,J.D. (2011) Integrative regulatory mapping indicates that the RNA-binding protein HuR couples pre-mRNA processing and mRNA stability. *Mol. Cell*, **43**, 327–339.
41. Lebedeva,S., Jens,M., Theil,K., Schwanhausser,B., Selbach,M., Landthaler,M. and Rajewsky,N. (2011) Transcriptome-wide analysis of regulatory interactions of the RNA-binding protein HuR. *Mol. Cell*, **43**, 340–352.
42. Wigington,C.P., Jung,J., Rye,E.A., Belauret,S.L., Philpot,A.M., Feng,Y., Santangelo,P.J. and Corbett,A.H. (2015) Post-transcriptional regulation of programmed cell death 4 (PDCD4) mRNA by the RNA-binding proteins human antigen R (HuR) and T-cell intracellular antigen 1 (TIA1). *J. Biol. Chem.*, **290**, 3468–3487.
43. Ule,J., Jensen,K., Mele,A. and Darnell,R.B. (2005) CLIP: a method for identifying protein-RNA interaction sites in living cells. *Methods*, **37**, 376–386.
44. Wigington,C.P., Morris,K.J., Newman,L.E. and Corbett,A.H. (2016) The polyadenosine RNA-binding protein, zinc finger Cys3His protein 14 (ZC3H14), regulates the Pre-mRNA processing of a key ATP synthase subunit mRNA. *J. Biol. Chem.*, **291**, 22442–22459.
45. Banerjee,A., Vest,K.E., Pavlath,G.K. and Corbett,A.H. (2017) Nuclear poly(A) binding protein 1 (PABPN1) and Matrin3 interact in muscle cells and regulate RNA processing. *Nucleic. Acids. Res.*, **45**, 10706–10725.
46. Blau,H.M., Pavlath,G.K., Hardeman,E.C., Chiu,C.P., Silberstein,L., Webster,S.G., Miller,S.C. and Webster,C. (1985) Plasticity of the differentiated state. *Science*, **230**, 758–766.
47. Lyons,G.E., Ontell,M., Cox,R., Sassoon,D. and Buckingham,M. (1990) The expression of myosin genes in developing skeletal muscle in the mouse embryo. *J. Cell Biol.*, **111**, 1465–1476.
48. Jainchill,J.L., Aaronson,S.A. and Todaro,G.J. (1969) Murine sarcoma and leukemia viruses: assay using clonal lines of contact-inhibited mouse cells. *J. Virol.*, **4**, 549–553.
49. Reich,E., Franklin,R.M., Shatkin,A.J. and Tatum,E.L. (1961) Effect of actinomycin D on cellular nucleic acid synthesis and virus production. *Science*, **134**, 556–557.
50. Lee,J.E., Lee,J.Y., Wilusz,J., Tian,B. and Wilusz,C.J. (2010) Systematic analysis of cis-elements in unstable mRNAs demonstrates that CUGBP1 is a key regulator of mRNA decay in muscle cells. *PLoS One*, **5**, e11201.
51. Herrick,D.J. and Ross,J. (1994) The half-life of c-myc mRNA in growing and serum-stimulated cells: influence of the coding and 3′ untranslated regions and role of ribosome translocation. *Mol. Cell. Biol.*, **14**, 2119–2128.
52. Barreau,C., Paillard,L. and Osborne,H.B. (2005) AU-rich elements and associated factors: are there unifying principles? *Nucleic Acids Res.*, **33**, 7138–7150.
53. Proudfoot,N.J. and Brownlee,G.G. (1976) 3′ non-coding region sequences in eukaryotic messenger RNA. *Nature*, **263**, 211–214.
54. Fitzgerald,M. and Shenk,T. (1981) The sequence 5′-AAUAAA-3′forms parts of the recognition site for polyadenylation of late SV40 mRNAs. *Cell*, **24**, 251–260.
55. Wickens,M. and Stephenson,P. (1984) Role of the conserved AAUAAA sequence: four AAUAAA point mutants prevent messenger RNA 3′ end formation. *Science*, **226**, 1045–1051.
56. Chen,C.Y. and Shyu,A.B. (1994) Selective degradation of early-response-gene mRNAs: functional analyses of sequence features of the AU-rich elements. *Mol. Cell. Biol.*, **14**, 8471–8482.
57. Peng,S.S., Chen,C.Y. and Shyu,A.B. (1996) Functional characterization of a non-AUUUA AU-rich element from the c-jun proto-oncogene mRNA: evidence for a novel class of AU-rich elements. *Mol. Cell. Biol.*, **16**, 1490–1499.
58. Apponi,L.H., Corbett,A.H. and Pavlath,G.K. (2011) RNA-binding proteins and gene regulation in myogenesis. *Trends Pharmacol. Sci.*, **32**, 652–658.
59. Ma,W.J., Chung,S. and Furneaux,H. (1997) The Elav-like proteins bind to AU-rich elements and to the poly(A) tail of mRNA. *Nucleic Acids Res.*, **25**, 3564–3569.
60. Fan,X.C. and Steitz,J.A. (1998) Overexpression of HuR, a nuclear-cytoplasmic shuttling protein, increases the in vivo stability of ARE-containing mRNAs. *EMBO J.*, **17**, 3448–3460.
61. Cammas,A., Sanchez,B.J., Lian,X.J., Dormoy-Raclet,V., van der Giessen,K., Lopez de Silanes,I., Ma,J., Wilusz,C., Richardson,J., Gorospe,M. *et al.* (2014) Destabilization of nucleophosmin mRNA by the HuR/KSRP complex is required for muscle fibre formation. *Nat. Commun.*, **5**, 4190.
62. Lee,J.H., Jung,M., Hong,J., Kim,M.K. and Chung,I.K. (2018) Loss of RNA-binding protein HuR facilitates cellular senescence through posttranscriptional regulation of TIN2 mRNA. *Nucleic Acids Res.*, **46**, 4271–4285.
63. Gherzi,R., Lee,K.Y., Briata,P., Wegmuller,D., Moroni,C., Karin,M. and Chen,C.Y. (2004) A KH domain RNA binding protein, KSRP, promotes ARE-directed mRNA turnover by recruiting the degradation machinery. *Mol. Cell*, **14**, 571–583.
64. Zhang,L., Lee,J.E., Wilusz,J. and Wilusz,C.J. (2008) The RNA-binding protein CUGBP1 regulates stability of tumor necrosis factor mRNA in muscle cells: implications for myotonic dystrophy. *J. Biol. Chem.*, **283**, 22457–22463.
65. Edwards,J.M., Long,J., de Moor,C.H., Emsley,J. and Searle,M.S. (2013) Structural insights into the targeting of mRNA GU-rich elements by the three RRMs of CELF1. *Nucleic Acids Res.*, **41**, 7153–7166.
66. Masuda,A., Andersen,H.S., Doktor,T.K., Okamoto,T., Ito,M., Andresen,B.S. and Ohno,K. (2012) CUGBP1 and MBNL1 preferentially bind to 3′ UTRs and facilitate mRNA decay. *Sci. Rep.*, **2**, 209.

67. van der Giessen,K., Di-Marco,S., Clair,E. and Gallouzi,I.E. (2003) RNAi-mediated HuR depletion leads to the inhibition of muscle cell differentiation. *J. Biol. Chem.*, **278**, 47119–47128.
68. Katsanou,V., Milatos,S., Yiakouvaki,A., Sgantzis,N., Kotsoni,A., Alexiou,M., Harokopos,V., Aidinis,V., Hemberger,M. and Kontoyiannis,D.L. (2009) The RNA-binding protein Elavl1/HuR is essential for placental branching morphogenesis and embryonic development. *Mol. Cell. Biol.*, **29**, 2762–2776.
69. Fan,X.C. and Steitz,J.A. (1998) HNS, a nuclear-cytoplasmic shuttling sequence in HuR. *Proc. Natl. Acad. Sci. U.S.A.*, **95**, 15293–15298.
70. von Roretz,C., Beauchamp,P., Di Marco,S. and Gallouzi,I.E. (2011) HuR and myogenesis: being in the right place at the right time. *Biochim. Biophys. Acta*, **1813**, 1663–1667.
71. Beauchamp,P., Nassif,C., Hillock,S., van der Giessen,K., von Roretz,C., Jasmin,B.J. and Gallouzi,I.E. (2010) The cleavage of HuR interferes with its transportin-2-mediated nuclear import and promotes muscle fiber formation. *Cell Death Differ.*, **17**, 1588–1599.
72. van der Giessen,K and Gallouzi,I.E. (2007) Involvement of transportin 2-mediated HuR import in muscle cell differentiation. *Mol. Biol. Cell*, **18**, 2619–2629.
73. Itoh,H., Tashima,Y., Eishi,Y. and Okeda,R. (1993) Localization of HSP90 in rat brain. *Int. J. Biochem.*, **25**, 93–99.
74. Srikakulam,R. and Winkelmann,D.A. (2004) Chaperone-mediated folding and assembly of myosin in striated muscle. *J. Cell Sci.*, **117**, 641–652.
75. Anantharaman,A., Tripathi,V., Khan,A., Yoon,J.H., Singh,D.K., Gholamalamdari,O., Guang,S., Ohlson,J., Wahlstedt,H., Ohman,M. *et al.* (2017) ADAR2 regulates RNA stability by modifying access of decay-promoting RNA-binding proteins. *Nucleic Acids Res.*, **45**, 4189–4201.
76. Chang,N., Yi,J., Guo,G., Liu,X., Shang,Y., Tong,T., Cui,Q., Zhan,M., Gorospe,M. and Wang,W. (2010) HuR uses AUF1 as a cofactor to promote p16INK4 mRNA decay. *Mol. Cell. Biol.*, **30**, 3875–3886.
77. Doller,A., Akool el,S., Huwiler,A., Muller,R., Radeke,H.H., Pfeilschifter,J. and Eberhardt,W. (2008) Posttranslational modification of the AU-rich element binding protein HuR by protein kinase Cdelta elicits angiotensin II-induced stabilization and nuclear export of cyclooxygenase 2 mRNA. *Mol. Cell. Biol.*, **28**, 2608–2625.
78. Mazan-Mamczarz,K., Galban,S., Lopez de Silanes,I., Martindale,J.L., Atasoy,U., Keene,J.D. and Gorospe,M. (2003) RNA-binding protein HuR enhances p53 translation in response to ultraviolet light irradiation. *Proc. Natl. Acad. Sci. U.S.A.*, **100**, 8354–8359.
79. Dormoy-Raclet,V., Cammas,A., Celona,B., Lian,X.J., van der Giessen,K., Zivojnovic,M., Brunelli,S., Riuzzi,F., Sorci,G., Wilhelm,B.T. *et al.* (2013) HuR and miR-1192 regulate myogenesis by modulating the translation of HMGB1 mRNA. *Nat. Commun.*, **4**, 2388.
80. Kim,H.H., Kuwano,Y., Srikantan,S., Lee,E.K., Martindale,J.L. and Gorospe,M. (2009) HuR recruits let-7/RISC to repress c-Myc expression. *Genes Dev.*, **23**, 1743–1748.
81. Abdelmohsen,K., Panda,A.C., Kang,M.J., Guo,R., Kim,J., Grammatikakis,I., Yoon,J.H., Dudekula,D.B., Noh,J.H., Yang,X. *et al.* (2014) 7SL RNA represses p53 translation by competing with HuR. *Nucleic Acids Res.*, **42**, 10099–10111.
82. Uren,P.J., Burns,S.C., Ruan,J., Singh,K.K., Smith,A.D. and Penalva,L.O. (2011) Genomic analyses of the RNA-binding protein Hu antigen R (HuR) identify a complex network of target genes and novel characteristics of its binding sites. *J. Biol. Chem.*, **286**, 37063–37066.
83. Abdelmohsen,K., Panda,A.C., Munk,R., Grammatikakis,I., Dudekula,D.B., De,S., Kim,J., Noh,J.H., Kim,K.M., Martindale,J.L. *et al.* (2017) Identification of HuR target circular RNAs uncovers suppression of PABPN1 translation by CircPABPN1. *RNA Biol.*, **14**, 361–369.